

# 1 Investigating small ion number size distributions: 2 insight into cluster formation and growth

3 Santeri Tuovinen<sup>1</sup>, Janne Lampilahti<sup>1</sup>, Nina Sarnela<sup>1</sup>, Chengfeng Liu<sup>1</sup>, Yongchun Liu<sup>2</sup> and Markku  
4 Kulmala<sup>1</sup> and Veli-Matti Kerminen<sup>1</sup>

5 <sup>1</sup>Institute for Atmospheric and Earth System Research/Physics, Faculty of Science, University  
6 of Helsinki, Helsinki, Finland

7 <sup>2</sup>Aerosol and Haze Laboratory, Beijing Advanced Innovation Center for Soft Matter Science  
8 and Engineering, Beijing University of Chemical Technology, Beijing, China

9  
10 Correspondence: Santeri Tuovinen (santeri.tuovinen@helsinki.fi) and Markku Kulmala  
11 (markku.kulmala@helsinki.fi)

## 12 Abstract

13 Small ions, consisting mostly of charged molecular clusters with mobility diameters below 2 nm,  
14 exist continuously in the atmosphere. Here, we studied small ion number size distributions  
15 measured with Neutral cluster and Air Ion Spectrometer measurements in Hyytiälä, Finland and  
16 Beijing, China. We found that in Hyytiälä, there is a strong positive relationship between the  
17 concentration and diameter of small ions of both polarities and highly oxidized organic molecule  
18 (HOM) and sulfuric acid concentrations, and that the relationship with the former is especially  
19 strong. The relationship between the negative sulfuric acid cluster ions and the small ion number  
20 size distribution in Hyytiälä was found to be more complex, but overall positive. In contrast to  
21 Hyytiälä, we found that in Beijing the small ion number size distribution does not have a clear  
22 relationship with sulfuric acid or oxidized organic molecule (OOM) concentration. We found that  
23 the small ion size distribution in Hyytiälä behaved as expected with respect to varying coagulation  
24 sink (CoagS), with concentrations of the smallest ions decreasing most with increasing CoagS.  
25 Surprisingly, the small ion size distribution in Beijing did not vary significantly with varying  
26 CoagS. However, in both locations, the impact of growth on the small ion number size distribution  
27 during periods of intense cluster formation and new particle formation is clearly seen. Our results  
28 show that while in Hyytiälä the growth of small ions to larger diameters is limited by the  
29 concentrations of sulfuric acid and OOMs, in Beijing there are additional factors required for the  
30 small ions to grow.

## 32 1 Introduction

33 Atmospheric aerosol particles influence the Earth's climate (e.g., Quaas et al., 2009; Boucher et al.,  
34 2013; Schmale et al., 2021; Li et al., 2022) and can have adverse effects on human health (e.g.,  
35 Shiraiwa et al., 2017; Arfin et al., 2023). These influences have commonly been related to  
36 properties, such as the mass or number concentration of an atmospheric aerosol population, its size  
37 distribution, or its chemical composition (Shiraiwa et al., 2017; Atkinson et al., 2015; Finlay, 2021).  
38 The electric charging state of atmospheric aerosols has attracted much less interest, although this  
39 property may have large influences on the dynamics of atmospheric aerosol populations (Harrison  
40 and Carslaw, 2003; Fdez-Arroyabe et al., 2022), thereby affecting many other important aerosol

41 properties. The presence of charges also makes it possible to measure low aerosol concentrations at  
42 high resolution in both time and particle size (Mirme and Mirme, 2013; Mirme et al., 2024).

43 Charged atmospheric particles, or more broadly ions, include charged aerosol particles, charged  
44 molecular clusters, and even large molecules having a charge. Ions with electrical mobility  
45 diameters roughly below 2 nm in diameter are classified as small ions, and consist of charged  
46 molecular clusters, while ions above 2 nm consist of charged aerosol particles (Tammet, 1995; Ehn  
47 et al., 2010). Of these charged aerosol particles, those with diameters between 2 and 7 nm are  
48 referred to as intermediate ions (Tammet, 1995).

49 Atmospheric ions are created through ionization of molecules the atmosphere. Most important of  
50 these ionization sources are cosmic ray radiation, gamma radiation, and radon decay (Harrison and  
51 Tammet, 2008). Small ions are constantly present in the troposphere as molecules are ionized and  
52 subsequently grow to small ions (Harrison and Tammet, 2008; Hirsikko et al., 2011). The lifetime of  
53 small ions is short at around 100 s, and their chemical composition depends on the atmospheric  
54 trace gas concentrations and their chemistry (Harrison and Tammet, 2008; Ehn et al., 2010; Shuman  
55 et al., 2015). In contrast, intermediate ions are typically detected mainly during the occurrence of  
56 atmospheric new particle formation (Tammet et al., 2014, Tuovinen et al., 2024), or during snowfall  
57 or rain (Hirsikko et al., 2007; Tammet et al., 2014). New particle formation (NPF) is considered to  
58 occur when constantly existing stable clusters, neutral or charged, start to grow to larger sizes by  
59 uptake of precursor vapors such as sulfuric acid and organic compounds with low volatilities  
60 (Kulmala et al., 2006; Kulmala et al., 2007; Lehtipalo et al., 2018; Kirkby et al., 2023).

61 A recent study by Kulmala et al. (2024a) presented the use of a novel cluster ion counter (CIC) for  
62 measuring small and intermediate ion concentrations to study local-scale NPF and to derive other  
63 parameters such as condensation sink (CS). The information gained by these measurements can be  
64 used further to study the complex climate-biosphere feedbacks (Kulmala et al., 2020; [Kulmala et al., 2024b](#)). These recent advances have motivated us to take a deeper look at the  
65 small ion size distribution.

67 The concentration of small ions depends on the ionization rate and the losses of small ions due to  
68 ion-ion recombination, coagulation with larger aerosol particles, and deposition (Tammet et al.,  
69 2006; Hörrak et al., 2008). The size of small ions depends on their chemical composition and age as  
70 the ions grow through chemical reactions and condensation of vapors, or through coagulation with  
71 neutral clusters. By investigating small ion number size distributions, we can learn more about these  
72 chemical and dynamical processes.

73 In this study, we combine ion number size distribution data measured by Neutral cluster and Air Ion  
74 Spectrometer (NAIS; Manninen et al., 2009; Mirme and Mirme, 2013) with concentrations of low-  
75 volatility vapors and ion clusters measured by mass spectrometer instruments to identify how, and  
76 why, the size distribution of small ions changes and evolves. Data from two different contrasting  
77 locations, Hyytiälä, Finland and Beijing, China (Kulmala et al., 2025), are used. First, we will study  
78 if the variation of the small ion size distribution with season is considerable. Secondly, we will  
79 quantify the potential relationship of organic low-volatility vapors and sulfuric acid on the size and  
80 number of small ions. [Third, we will analyze the impact of coagulation scavenging on small ion size  
81 distribution.](#) ~~Fourth~~ [Thirdly](#), we will analyze the small ion size distribution as a function of intensity  
82 of NPF to reveal how the small ion size distribution changes as the clusters grow. Finally, some case

83 studies are presented. With these, we aim to identify the most important processes impacting the  
84 small ion number size distribution, and to evaluate the role of these processes in driving the growth  
85 of small ions to intermediate ions.

## 86 2 Background and methods

### 87 2.1 Evolution of small ion size distribution

88 Typically, the parameter of interest when considering small ions is their total number concentration  
89 and its temporal evolution. The changing in the small ion number concentration can be described  
90 by the simplified air ion balance equation:

$$\frac{dN^\pm}{dt} = Q - CoagS N^\pm - \alpha N^\pm N^\mp - S N^\pm \quad (1)$$

91 Here,  $N^\pm$  is the concentration of one polarity, while  $N^\mp$  is the concentration of the other polarity.  
92 The first term on the right-hand side of the equation describes the source rate of the ions, where  $Q$  is  
93 the ionization rate of air molecules. The second term, where CoagS stands for coagulation sink,  
94 tells the loss rate of small ions due to coagulation on larger aerosol particles. The third term tells the  
95 loss rate of ions due to ion-ion recombination, where  $\alpha$  is the ion recombination coefficient. The  
96 final term describes other losses of the ions, including deposition, and  $S$  is the loss rate of the ions to  
97 these other sinks.

98  
99 As we can see, the above equation does not explicitly depend on the size of the small ions nor can it  
100 be directly used to describe the evolution of the size-dependent small ion size distribution. The time  
101 evolution of small ions of certain size  $i$  are described by the charged general dynamics equations  
102 (charged GDEs; Kulmala et al., 2012):

$$\frac{dN_i^\pm}{dt} = J_i + \chi N_i N_{d<i}^\pm - N_i^\pm CoagS_i - \alpha N_i^\pm N_{d<i}^\mp - \frac{GR}{\Delta d_i} N_i^\pm \quad (2)$$

103 Here,  $J_i$  is the formation rates of ions of size  $i$ . The second term on the right-hand side represents the  
104 charging of neutral clusters by ions smaller than  $i$ , where  $\chi$  is the ion-cluster attachment coefficient.  
105 The last term, where GR is the ion growth rate, describes the growth of ions  $i$  to larger sizes.  
106 Considering Eq. 2, we can see that an increasing GR will shift the ion size distribution towards  
107 larger diameters. CoagS is the highest for the smallest ions and if it increases, the concentrations of  
108 smallest ions are decreasing the most, causing an apparent shift in the distribution towards larger  
109 diameters. However, CoagS also affect the lifetime of small ions, so that with an increasing CoagS  
110 the ions have less time to grow, reducing the concentration of larger small ions. If ion  
111 concentrations are high, ion-ion recombination rate will be higher, which will also lead to shorter  
112 small ion lifetime and possibly smaller concentrations of larger small ions. Through ion-cluster  
113 attachment, the small ion size distribution depends on the size distribution of neutral clusters,  
114 although this term is relatively small when compared to the coagulation loss and growth terms.

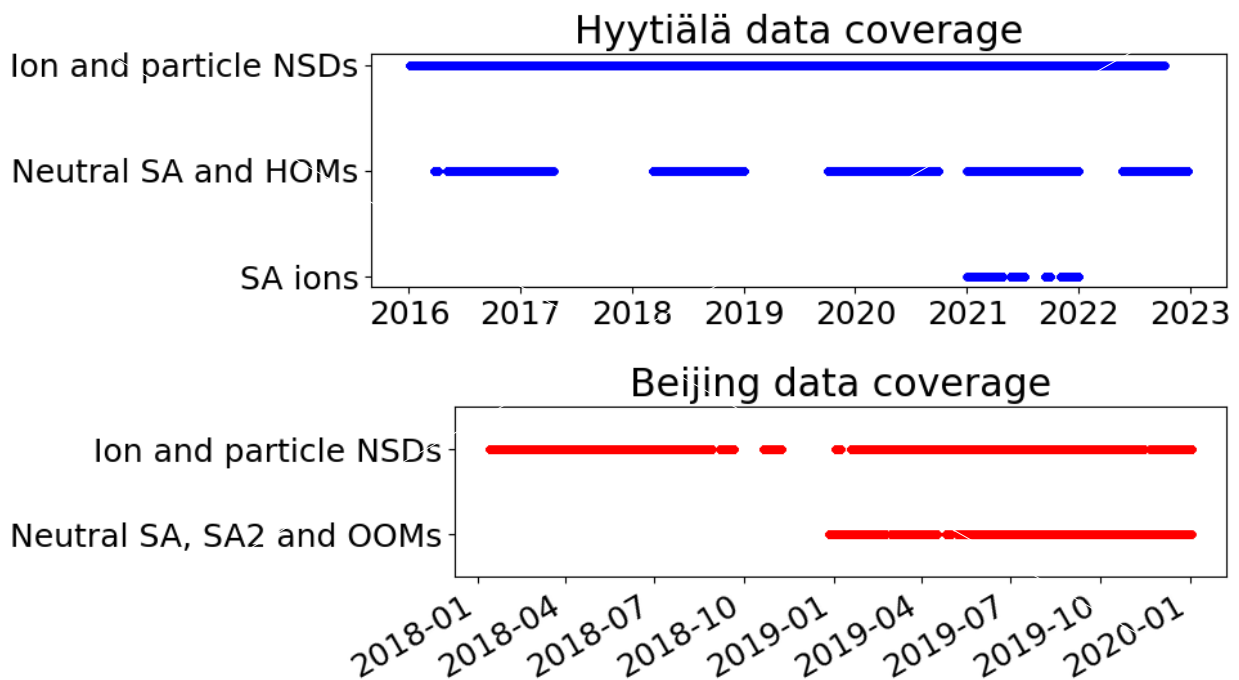
115 We assume that the role of direct transport of clusters on the changes in the small ion size  
116 distribution is negligible due to their short lifetime of just a couple of minutes (Tamm et al.,  
117 2006). Therefore, the observations are assumed to be very local. However, transport can indirectly  
118 impact the size distribution of small ions i.e., through transport of trace gases and larger particles.  
119 We also note that while meteorological conditions, such as temperature, strongly influence  
120 processes such as HOM formation (e.g., Quéléver et al., 2019), we do not explicitly consider them

121 | ~~in this study. In this study, we are mainly interested in the formation and growth of ions, and their~~  
122 | ~~impacts on the small ion size distribution. Impacts of coagulation scavenging or ion-ion~~  
123 | ~~recombination on the small ion size distribution are not explicitly considered in this study.~~

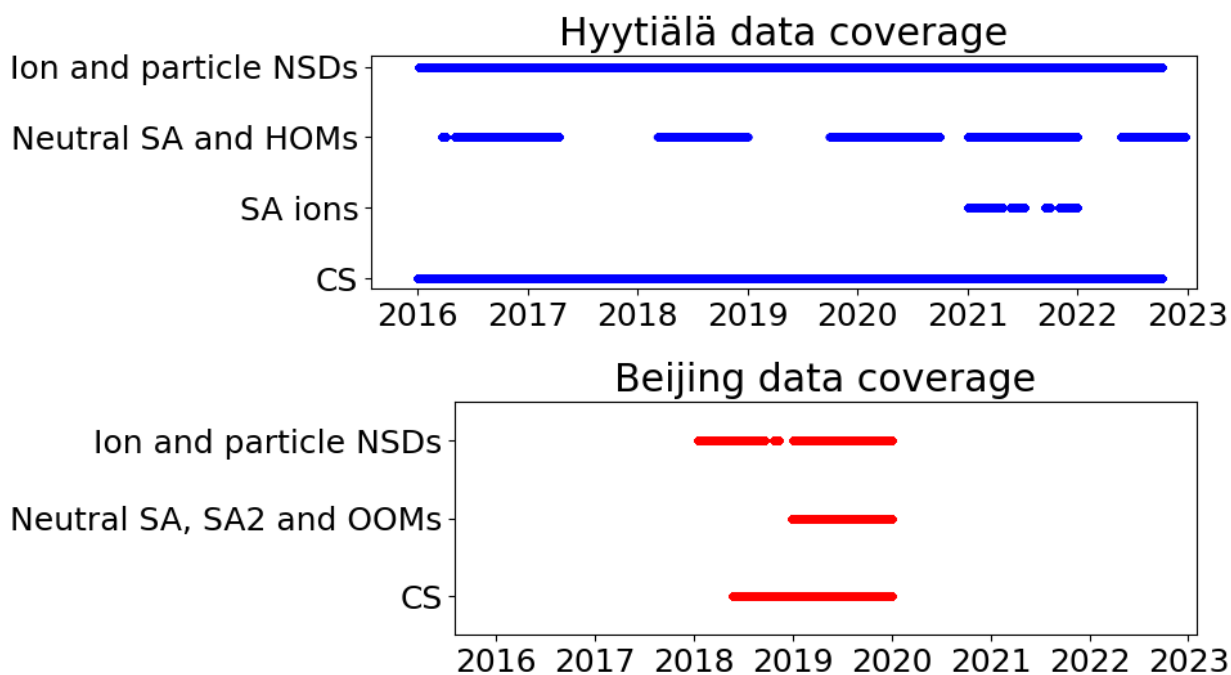
## 124 | 2.2 Measurement sites

125 | Two different locations were considered in this study: SMEAR II measurement station in Hyytiälä,  
126 | Finland (61°51' N, 24°17' E) and BUCT/AHL measurement station in Beijing, China (39°94' N,  
127 | 116°30' E). The former is a rural site surrounded by boreal forest while the latter is an urban site  
128 | close to residential building and traffic roads. For more details on SMEAR II station, see Hari and  
129 | Kulmala. (2005). For more details on BUCT/AHL site, see Liu et al. (2020). These two locations  
130 | are included in the analysis due to their contrasting natures, providing an opportunity for insight  
131 | into the variation of small ion size distribution and small ion dynamics in different environments.

## 132 | 2.3 Measurement and other data



133



134  
 135 **Fig.1:** Data coverage for the two sites, Hyytiälä, Finland, and Beijing, China, from which data  
 136 were used in this study. NSD refers to number size distribution, while SA refers to sulfuric acid,  
 137 SA2 to neutral sulfuric acid dimer, HOM to highly oxidized organic molecule and OOM to oxidized  
 138 organic molecule.

139  
 140 Atmospheric ion and total particle number size distributions in Hyytiälä and Beijing were measured  
 141 with Neutral cluster and Air Ion Spectrometer (NAIS; Manninen et al., 2009; Mirme and Mirme,  
 142 2013). The NAIS measures both charged and total particle number size distributions in the ranges  
 143 0.8-42 nm and 2.5–42 nm, respectively. Main focus of the analysis in this study is on the number  
 144 size distributions of small ions (diameters below 2 nm). Ion concentrations between 2.0 and 2.3 nm  
 145 were used to characterize the intensity of local clustering (Tuovinen et al., 2023) and new particle  
 146 formation ranking data, characterizing the intensity of NPF, were also used. The NPF ranking was  
 147 based on the total particle number concentration between 2.5 and 5 nm and determined according to  
 148 the method presented by Aliaga et al. (2023).

149 The chemical composition of small ions typically differs between the polarities (Ehn et al., 2010;  
 150 Zha et al., 2023). For example, Ehn et al. (2010) found that in Hyytiälä the daytime negative small  
 151 ions consisted largely of sulfuric acid clusters, while positive small ions consisted of organic species  
 152 such as alkyl pyridines and alkyl amines. Therefore, we cannot assume that the negative and  
 153 positive small ion populations behave similarly with respect to i.e., increased sulfuric acid  
 154 concentrations. Thus, both negative and positive polarity were separately considered.

155 All diameters used in study are electrical mobility diameters. We note that especially for the  
 156 smallest of the ions the mobility diameter may not accurately describe the physical dimensions of  
 157 the ion (see e.g., Ehn et al., 2011). Regardless, we refer to diameter rather than electrical mobility as  
 158 we see it as more intuitively understandable parameter for the ion size.

159 From Hyytiälä, concentrations of neutral sulfuric acid and highly oxidized organic molecules  
 160 (HOMs) were used to study the influence of cluster formation and growth on the small ion size  
 161 distribution. These were measured with Chemical Ionization Atmospheric Pressure interface Time-

162 Of-Flight (CI-API-TOF) mass spectrometer (Jokinen et al., 2012). In addition, the signal counts of  
163 ionized sulfuric acid clusters measured with API-TOF were used to give further insight into the  
164 composition of the small ions. The signal counts in the study are given as relative signals to the total  
165 measured ion current. From Beijing, neutral sulfuric acid, sulfuric acid dimer and total oxidized  
166 organic molecule (OOM) concentrations, which were measured with a nitrate based – long time-of-  
167 flight chemical ionization mass spectrometer (CIMS), were included in the analysis. We note that  
168 we use the term OOM instead of HOM for the organic molecules in Beijing based on previous  
169 results by Yan et al. (2021), suggesting that most of these measured organic molecules in Beijing do  
170 not meet the requirements for HOMs (see Bianchi et al., 2019).

171  
172 Condensation sinks (CS) for both sites were included in the analysis as proxies for the coagulation  
173 scavenging of the small ions. In Hyytiälä, the particle size distributions from which CS was derived  
174 from were measured with a twin Differential Mobility Particle Sizer (DMPS) system (Aalto et al.,  
175 2001). In Beijing, the particle size distributions for CS were measured with a particle size  
176 distribution (PSD) system (Liu et al., 2016).

177  
178 Data coverage for both sites is presented in Fig. 1.  
179

## 180 2.4 Determining the average small ion diameter

181 From the small ion number size distributions, we determined the mean mobility diameter ( $d_{\text{mean}}$ ),  
182 and median mobility diameter ( $d_{\text{median}}$ ) of small ions. First, cubic interpolation was applied to the  
183 measured ion number size distributions. We note that nearest neighbor and linear interpolation  
184 methods were also tested, and the influence of the chosen method on the value of  $d_{\text{mean}}$  or  $d_{\text{median}}$  was  
185 found minor. The diameter range for the interpolation was from the lower detection limit to 2 nm  
186 with a step of 0.001 nm. Then,  $d_{\text{peak}}$  was determined by finding the diameter corresponding to the  
187 maximum concentration of small ions. Weighted mean and median were used to determine  $d_{\text{mean}}$  and  
188  $d_{\text{median}}$ , with the number concentrations of ions below 2 nm in diameter used as weights. The  
189 equation below was used to find weighted mean diameter:

$$190 \quad d_{\text{mean}} = \frac{\sum N_i d_i}{\sum N_i}, \quad (3)$$

191 where  $d_i$  is the diameter of ions of a certain size and  $N_i$  is their number concentration. The weighted  
192 median was determined by finding the diameter  $d_j$  satisfying

$$193 \quad j = \min_k \left[ \sum N_i d_i > \frac{1}{2} \sum N_i d_i \right]. \quad (4)$$

194  
195

## 196 3 Results

### 197 3.1 Seasonal variation of the small ion size distribution

#### 198 3.1.1 Hyytiälä

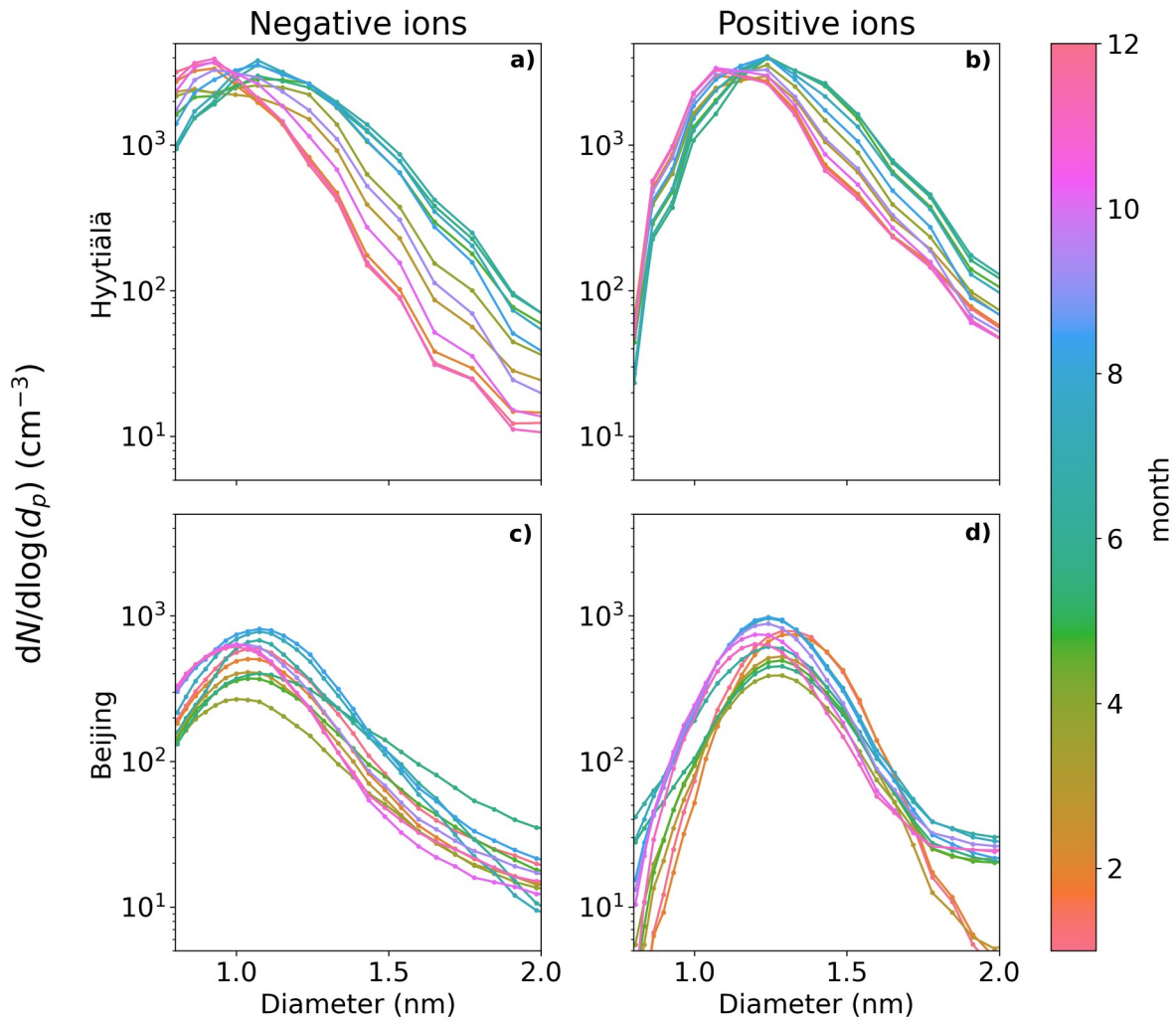
199 The ~~upper panel of~~ Fig. 2a and b shows the monthly median negative and positive ion distributions  
200 between 0.8 and 2 nm in Hyytiälä. Table 12 records the monthly mean and median diameters ( $d_{\text{mean}}$   
201 and  $d_{\text{median}}$ ). Clear month-to-month changes in the size distributions are observed, and these are  
202 more pronounced for negative ions (Fig. 2a). During winter, the concentration of negative ions

203 | peaks already below 1.0 nm, while during summer the highest concentration is between 1.1 and 1.2  
204 | nm. In addition, the concentrations of negative ions above 1.1 nm are increased from winter to  
205 | summer. Close to 2 nm, the ion concentration is almost one order of magnitude higher during  
206 | summer. This behavior of the size distribution is reflected in the values of  $d_{\text{mean}}$  and  $d_{\text{median}}$ , which are  
207 | smallest during December and January, with  $d_{\text{mean}} = 0.99$  nm and  $d_{\text{median}} = 0.95$  nm, and the largest  
208 | during June and July, with  $d_{\text{mean}} = 1.15$  nm and  $d_{\text{median}} = 1.11$  nm.

209 | Positive ion size distributions (Fig. 2b) behave similarly ~~to theas the~~ negative ones, however the  
210 | changes are less pronounced. Above 1.4 nm and up to 2.0 nm, the concentrations are roughly twice  
211 | as high, or less, during summer compared to winter. For positive small ions, the smallest value of  
212 |  $d_{\text{mean}} = 1.16$  and  $d_{\text{median}} = 1.13$  nm (December and January) and the largest value of  $d_{\text{mean}} = 1.29$  nm  
213 | and  $d_{\text{median}} = 1.27$  nm (June). The difference between the average diameters of negative and positive  
214 | small ions was around 0.15 nm, in line with previous studies (e.g., Hörrak et al., 2000).

215 | The observed seasonal behavior of the size distributions in Hyttiälä follow expectations: during  
216 | spring and summer, the concentrations of low-volatility vapors are much higher due to increased  
217 | solar radiation and organic emissions (Sulo et al., 2021). Therefore, small ions should be able to  
218 | grow to larger diameters due to the uptake of these vapors. We will look further into how the small  
219 | ion size distribution varies with respect to low volatile vapor concentrations in Sect. 3.2.

220 | [3.1.2 Beijing](#)



221  
 222 **Fig. 2:** Median monthly sub-2 nm negative (a, cleft) and positive (b, dright) ion size distributions  
 223 for Hyytiälä (a, btop) and Beijing (c, dbottom). The different months are marked by the different  
 224 colors.

225  
 226 The bottom panel of Fig. 2c, d shows the monthly median negative (Fig. 2c) and positive (Fig. 2d)  
 227 ion distributions between 0.8 and 2.0 nm in Beijing, while Table 23 records the monthly  $d_{\text{mean}}$  and  
 228  $d_{\text{median}}$ . As expected due to the high CoagS (Eq. 1,2, and Fig. A1), the concentrations are lower than  
 229 in Hyytiälä. Compared to Hyytiälä, the seasonal trends in Beijing are much more unclear and  
 230 complex. For negative ions (Fig. 2c), the concentrations during summer are higher than in other  
 231 seasons below 1.6 nm and lower than in other seasons close to 2.0 nm. During spring, the  
 232 concentrations of negative ions below 1.4 nm are lower than in other seasons. The smallest value of  
 233 negative  $d_{\text{mean}}$  and  $d_{\text{median}}$  are in November,  $d_{\text{mean}} = 1.04$  nm and  $d_{\text{median}} = 1.01$  nm. The largest values  
 234 are during June,  $d_{\text{mean}} = 1.16$  nm and  $d_{\text{median}} = 1.12$  nm.

235 For positive small ions in Beijing (Fig. 2d), the concentrations of both the smallest and the largest  
 236 ions in the 0.8 to 2.0 nm range close to 0.8 nm and 2 nm are both considerably lower from January  
 237 to March compared to later months. Otherwise, it is difficult to identify any clear seasonal patterns.  
 238 The largest positive average diameter is during February,  $d_{\text{mean}} = 1.32$  nm and  $d_{\text{median}} = 1.31$  nm,  
 239 while the smallest values are in November,  $d_{\text{mean}} = 1.22$  nm and  $d_{\text{median}} = 1.21$  nm.

240 | Compared to Hyytiälä, the seasonal trends in Beijing are much less clear, which implies that the  
 241 | factors controlling the small ion size distribution are less seasonal in Beijing than in Hyytiälä, where  
 242 | the small ion size distribution show strong seasonal variation. However, wWe note that because  
 243 | there are less data from Beijing compared to Hyytiälä, variation between years can have larger  
 244 | impact on the results than in Hyytiälä.

245 |  
 246 | **Table 1:** Mean and median monthly diameters (nm) of ions between 0.8 and 2.0 nm in Hyytiälä.  
 247 | \*The highest concentration corresponds to the lowest detected diameter.

Month	Negative ions		Positive ions	
	$d_{\text{mean}}$	$d_{\text{median}}$	$d_{\text{mean}}$	$d_{\text{median}}$
1	0.99	0.95	1.16	1.13
2	1.00	0.96	1.17	1.15
3	1.05	1.02	1.2	1.18
4	1.08	1.06	1.21	1.20
5	1.12	1.10	1.27	1.25
6	1.15	1.11	1.29	1.27
7	1.15	1.11	1.28	1.26
8	1.13	1.10	1.25	1.23
9	1.11	1.08	1.22	1.20
10	1.05	1.02	1.19	1.17
11	1.01	0.98	1.17	1.14
12	0.99	0.95	1.16	1.13

248 |  
 249 |  
 250 | **Table 2:** Mean and median monthly diameters (nm) of ions between 0.8 and 2.0 nm in Beijing.  
 251 | \*The highest concentration corresponds to the lowest detected diameter.

Month	Negative ions		Positive ions	
	$d_{\text{mean}}$	$d_{\text{median}}$	$d_{\text{mean}}$	$d_{\text{median}}$
1	1.10	1.07	1.30	1.30
2	1.09	1.06	1.32	1.31
3	1.09	1.06	1.28	1.27
4	1.10	1.05	1.28	1.26
5	1.12	1.07	1.28	1.27
6	1.16	1.12	1.27	1.26
7	1.12	1.08	1.25	1.24
8	1.10	1.08	1.25	1.24

9	1.10	1.07	1.25	1.24
10	1.07	1.03	1.24	1.23
11	1.04	1.01	1.22	1.21
12	1.05	1.01	1.23	1.21

252

253

## 254 **3.2 Potential impact of low volatility vapors to small ion size distribution** 255 **in Hyytiälä**

### 256 **3.2.1 Highly oxidized organic molecules (HOMs)**

257 Fig. 3 shows the median ion number size distributions between 0.8 and 2.0 nm in Hyytiälä with  
258 respect to varying neutral highly oxidized organic molecule (HOM) concentration. HOM  
259 monomers, HOM dimers and total HOM are considered separately. Results for daytime (10:00-  
260 16:00) and evening (18:00-00:00) are both presented (Fig. 3a and 3b, respectively). The HOM  
261 concentrations are divided into percentiles.

262 A clear increase in the number of negative ions (Fig. 3a, i-iii, Fig. 3b, i-iii) above approx. 1.05 nm,  
263 and for positive ions (Fig. 3a, iv-vi, Fig. 3b, iv-vi) slightly larger than that, is seen with an  
264 increasing HOM concentration percentile for all the plotted HOM categories. The difference is the  
265 largest for HOM monomers (i, iv) and HOM total (iii, vi), which is mainly dominated by the HOM  
266 monomers. The difference is also stronger for negative ions than positive ions, and is stronger  
267 during the evening (Fig. 3b) compared to daytime (Fig. 3a).

268 Comparing the negative ion size distributions between the HOM percentiles of 0-20% and 80-  
269 100%, we see that the difference in the concentrations increases with an increasing diameter, and  
270 that close to 2.0 nm this difference is approximately one order of magnitude during daytime (Fig.  
271 3aa,i-iii) and a bit more than that during the evening (Fig. 3bb, i-iii). ~~The negative ion size~~  
272 ~~distributions for different HOM percentiles are otherwise quite similar during the daytime and~~  
273 ~~evening, however during the evening the difference between the respective size distributions for~~  
274 ~~HOM monomer percentile 60-80% and 80-100% is higher (Fig. 3b). During daytime, the ion~~  
275 ~~concentrations are similar in the 60-80% and 80-100% percentiles (Fig. 3a), while during the~~  
276 ~~evening, the concentration close to 2 nm is around twice as high when HOM monomer~~  
277 ~~concentration is in the 80-100% percentile compared to 60-80% percentile (Fig. 3b).~~ Comparing the  
278 similar negative ion concentrations when HOM monomer concentration during the evening is in the  
279 80-100% percentile compared to 0-20%, there's approx. a 0.5 nm shift in diameters (Fig. 3b, i),  
280 which is a bigmajor difference for the sub-2 nm ion population.

281 In line with the large differences in the small ion size distributions in Fig. 3 with respect to HOM  
282 concentration, a strong correlation between the small ion  $d_{\text{mean}}$  and the HOM concentrations was  
283 seen (Fig. 4). The Spearman correlation coefficients ( $r_s$ ) between  $d_{\text{mean}}$  and HOMs were 0.6 or  
284 above, for both daytime and evening. For daytime, the best correlation was between  $d_{\text{mean}}$  of positive  
285 ions and HOM monomer concentration,  $r_s = 0.74$  (Fig. 4e). During nighttime, the strongest  
286 correlation was between  $d_{\text{mean}}$  of negative ions and HOM- monomer concentration,  $r_s = 0.73$  (Fig.

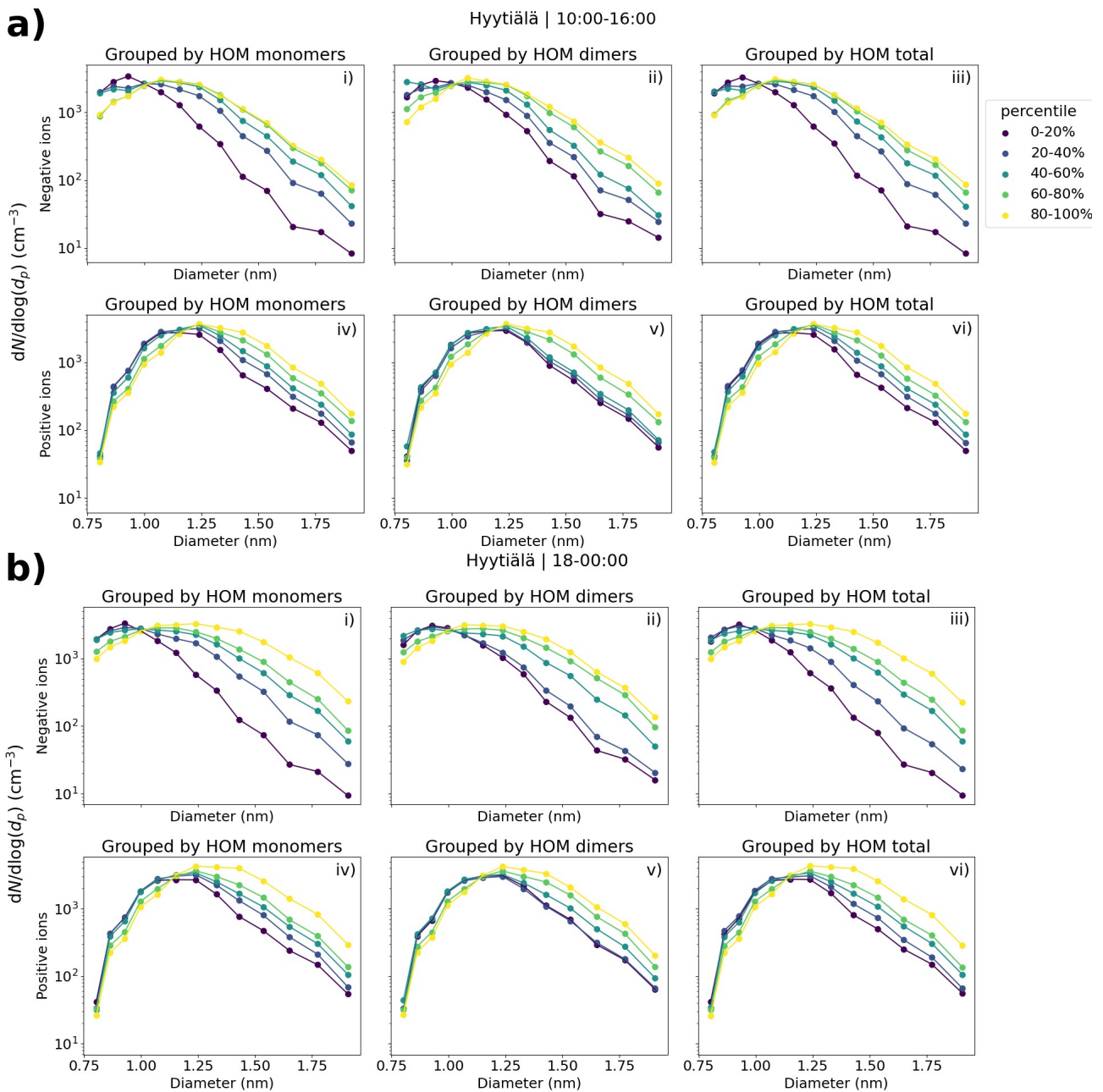
287 | ~~4c). By using a variable such as  $d_{\text{mean}}$ , we have been able to get some insight about the behavior of~~  
288 | ~~the underlying ion size distribution.~~

289 | The clear correlation between HOMs and the small ion size distribution in Hyytiälä suggests a  
290 | strong impact of organic compounds to the small ion population. This interpretation, as opposed to  
291 | the correlation being due to a correlation with another variable such sulfuric acid concentration, is  
292 | supported by the observation of the correlation being stronger during evening when the  
293 | concentrations of other precursors such as sulfuric acid are lower and organic ion cluster formation  
294 | is known to take place in Hyytiälä (Mazon et al., 2016; Rose et al., 2018). We note that pPart of the  
295 | increase in the diameters of the small ions when HOMs are abundant could be due to the large size  
296 | of organic molecules when compared to sulfuric acid molecules. However, the clear increase in  
297 | concentrations even close to 2.0 nm suggests that ~~a significant part of~~ the impact is mainly due to  
298 | the growth of small ions by the uptake of organic vapors.

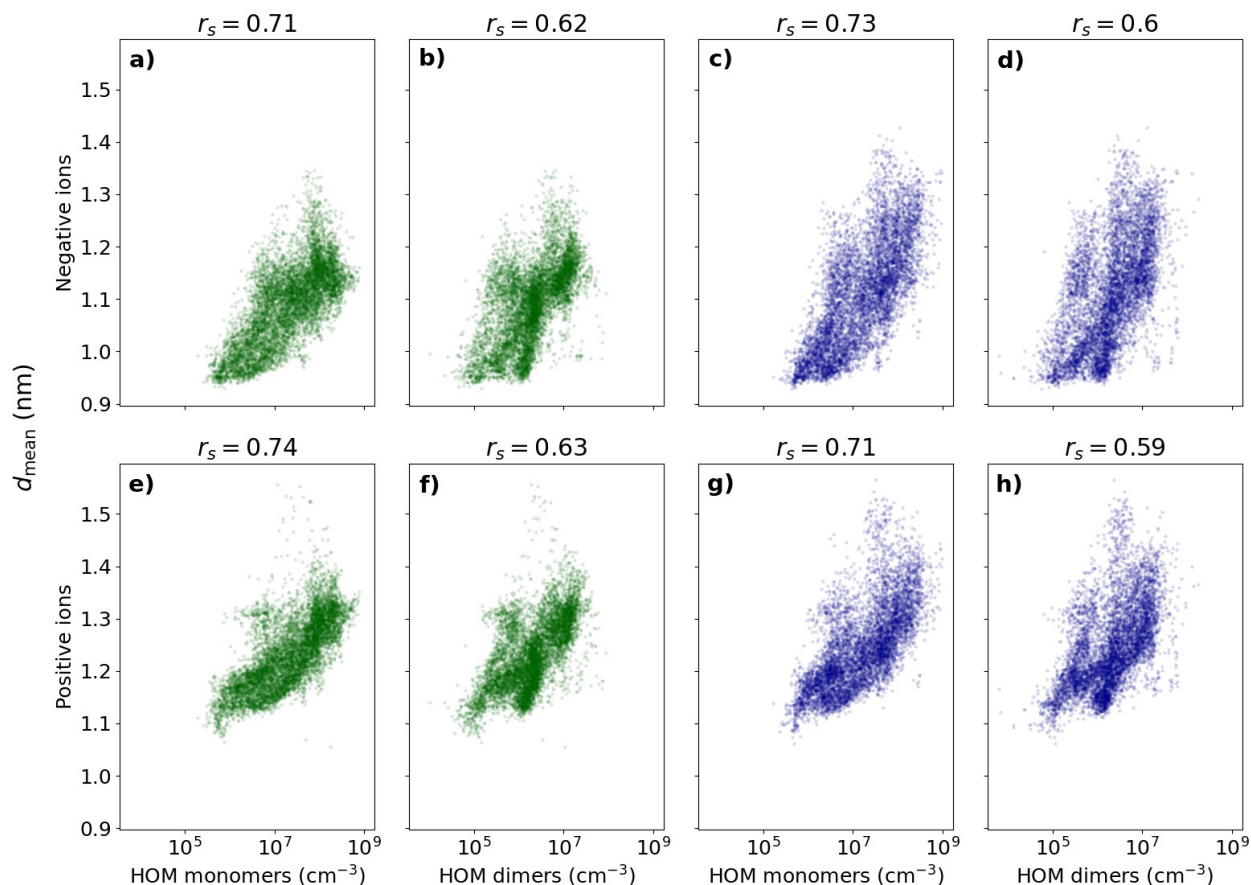
299 | While the concentrations of larger small ions of both polarities increase with increasing HOM  
300 | percentile, the differences are larger for the negative ions (Fig. 3). This could be due to the uptake  
301 | of organics being more effective for the negatively charged ions. However, the equally strong  
302 | correlation between  $d_{\text{mean}}$  of positive small ions and HOM concentrations does not support this  
303 | interpretation. A possible explanation is the size difference between the negative and positive small  
304 | ions: due to the larger diameter of positive small ions, it might be that the impact of the growth to  
305 | the diameters of the positive ions is not as large. For a larger cluster (ion), more molecules are  
306 | needed to increase the diameter equally than for a smaller one.

307 |

308 |



309  
 310 **Fig. 3:** The median negative (i-iii) and positive (iv-vi) small ion (sub-2 nm) size distributions in  
 311 Hyytiälä, Finland grouped by the percentiles of neutral HOM monomer (i, iv), HOM dimer (ii, v)  
 312 and total HOM (iii, vi) concentrations. Both the evening (18:00-00:00) size distributions (b) and  
 313 daytime (10:00-16:00) size distributions (a) are shown. Daytime percentiles for HOM monomers,  
 314 dimers and total are 20%:  $4.30 \cdot 10^6$ ,  $5.93 \cdot 10^5$ , and  $5.10 \cdot 10^6$   $\text{cm}^{-3}$ ; 40%:  $1.34 \cdot 10^7$ ,  $1.45 \cdot 10^6$ , and  
 315  $1.50 \cdot 10^7$   $\text{cm}^{-3}$ ; 60%:  $4.00 \cdot 10^7$ ,  $2.44 \cdot 10^6$ , and  $4.18 \cdot 10^7$   $\text{cm}^{-3}$ ; 80%:  $9.70 \cdot 10^7$ ,  $7.62 \cdot 10^6$ , and  $1.05 \cdot 10^8$   $\text{cm}^{-3}$ ,  
 316 respectively. Evening percentiles for HOM monomers, dimers and total are 20%:  $3.00 \cdot 10^6$ ,  
 317  $4.94 \cdot 10^5$ , and  $3.75 \cdot 10^6$   $\text{cm}^{-3}$ ; 40%:  $8.40 \cdot 10^6$ ,  $1.50 \cdot 10^6$ , and  $1.03 \cdot 10^7$   $\text{cm}^{-3}$ ; 60%:  $3.17 \cdot 10^7$ ,  $2.95 \cdot 10^6$ ,  
 318 and  $3.65 \cdot 10^7$   $\text{cm}^{-3}$ ; 80%:  $7.52 \cdot 10^7$ ,  $7.70 \cdot 10^6$ , and  $8.46 \cdot 10^7$   $\text{cm}^{-3}$ , respectively.



319  
 320 | **Fig. 4:** Mean diameter ( $d_{\text{mean}}$ ) of negative positive (a-d) and positive (e-h) negative small (sub-2 nm)  
 321 ions as a function of HOM (monomer, dimer and total) concentration in Hyytiälä. The individual  
 322 points are hourly medians, and the daytime (10:00-16:00, marked in green) and evening (18:00-  
 323 00:00, marked in dark blue) are shown separately. Spearman correlation coefficients ( $r_s$ ) are shown.  
 324

### 325 3.2.2 Sulfuric acid

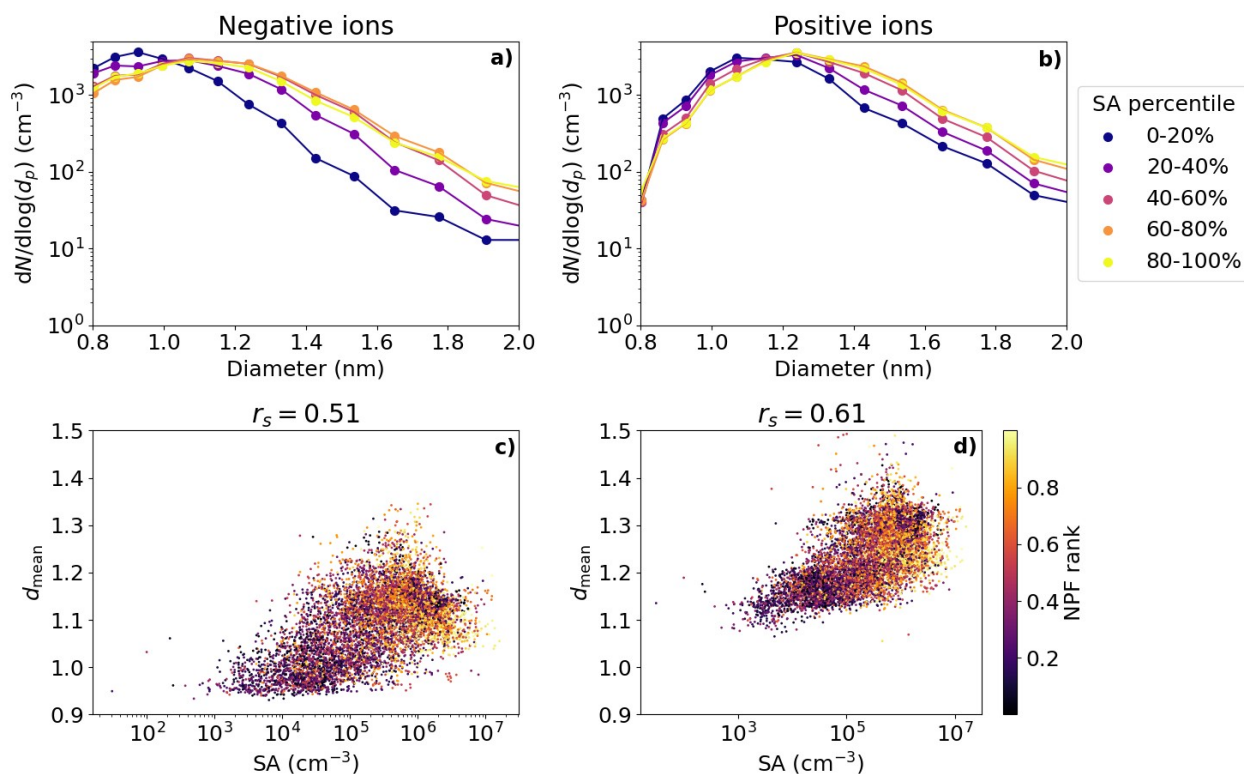
326 Fig. 5 shows the median daytime negative and positive small ion (0.8-2.0 nm) size distributions  
 327 grouped by percentiles of neutral sulfuric acid (SA) concentration (Fig. 5a and b), ~~add percentiles~~  
 328 ~~here~~. In addition, the daytime hourly median  $d_{\text{mean}}$  values are shown as a function of the SA  
 329 concentration (Fig. 5c and d). We see a clear increase in the concentrations of negative (positive)  
 330 small ions larger than approximately 1.05 (1.1) nm when comparing SA concentrations in the lower  
 331 percentiles to the higher percentiles, until the behavior seems to stall so that the 60-80% and 80-  
 332 100% percentiles show similar size distributions. From previous studies, we know that while  
 333 sulfuric acid is often needed for the initial cluster formation, organic compounds tend to drive the  
 334 cluster growth (Kulmala et al., 2013). This ~~might could partially~~ explain the small difference in the  
 335 size distributions between the 60-80% and 80-100% percentiles of the SA concentration.

336 A good positive correlation was seen between  $d_{\text{mean}}$  and SA concentration for both polarities,  $r_s =$   
 337 0.51 (0.61) for negative (positive) ions (Fig. 5c and d). The correlation is slightly weaker than what  
 338 was observed between  $d_{\text{mean}}$  and HOM, especially monomer, concentrations. The majority of  $d_{\text{mean}}$   
 339 values above 1.1 nm correspond to days with a high NPF ranking, while most values of  $d_{\text{mean}}$  below  
 340 1.1 nm correspond to days with low NPF rank values below 0.5. Notably, for  $d_{\text{mean}}$  of negative small

341 ions above approx. 1.1 nm, the values of  $d_{\text{mean}}$  do not seem to increase with an increasing SA  
 342 concentration as clearly as they do with an increasing HOM concentration (Fig. 4) . As discussed  
 343 above, organic compounds might be needed to drive the growth of small ions further, and thus  
 344 dependency of  $d_{\text{mean}}$  on SA is not seen as clearly when  $d_{\text{mean}}$  is above 1.1 nm.

345

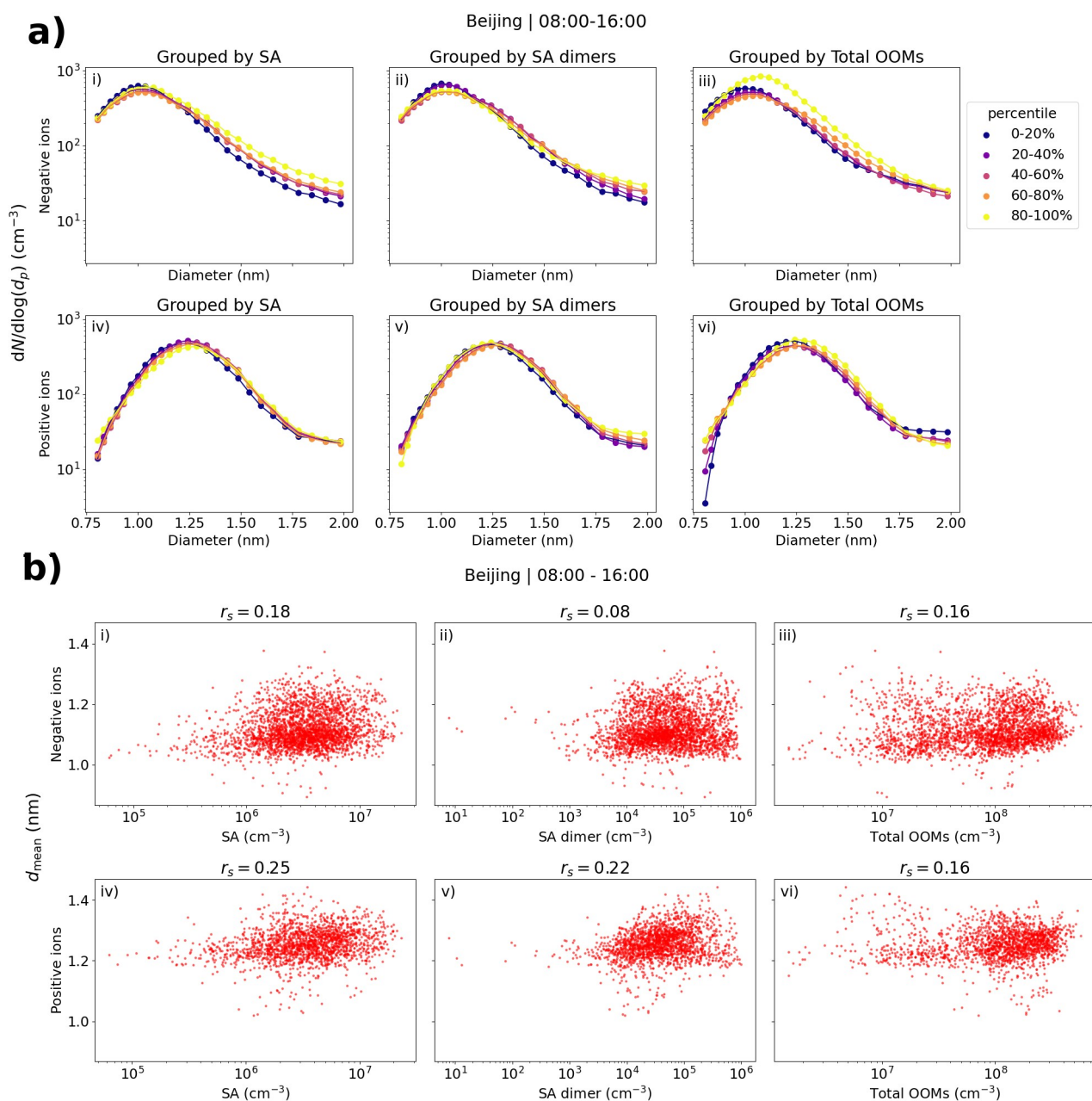
Hyytiälä | 10:00 - 16:00



346

347 **Fig. 5:** The median number size distributions of small ions between 0.8 and 2.0 nm grouped by  
 348 percentiles of neutral sulfuric acid concentration (a) negative and b) positive ions)percentiles; top  
 349 panel) and scatter plots and Spearman correlation coefficients ( $r_s$ ) of hourly mean diameter of small  
 350 ions ( $d_{\text{mean}}$ ) and sulfuric acid concentration (c) negative and d) positive ionsbottom panel) in  
 351 Hyytiälä. In the scatter plot, the color indicates the respective NPF rank of the day. Only daytime  
 352 (10:00-16:00) values are included. The percentile values for sulfuric acid are 20%:  $4.22 \cdot 10^4$  cm<sup>-3</sup> ,  
 353 40%:  $1.79 \cdot 10^5$  cm<sup>-3</sup> , 60%:  $5.06 \cdot 10^5$  cm<sup>-3</sup> and 80%:  $1.08 \cdot 10^6$  cm<sup>-3</sup>.

354 **3.3 Relationship of small ion size distribution with low volatility vapors**  
 355 **in Beijing**



356 **Fig. 6:** (a) Small ion median daytime (08:00-16:00) number size distributions in Beijing, grouped  
 357 by percentiles of sulfuric acid (SA), SA dimer or total oxidized organic molecule (OOM)  
 358 concentrations. (b) Hourly daytime mean diameter ( $d_{\text{mean}}$ ) of small ions versus SA, SA dimer and  
 359 total OOM concentrations. Figures i-iii are for negative polarity and figures iv-vi for positive and  
 360 the figures with SA, SA dimer, and OOMs are in the respective order. Spearman correlation  
 361 coefficients ( $r_s$ ) are included. The percentile limits of SA, SA dimer and total OOM are 20%:  
 362 1.64·10<sup>6</sup>, 1.26·10<sup>4</sup>, and 2.19·10<sup>7</sup> cm<sup>-3</sup>; 40%: 2.53·10<sup>6</sup>, 3.11·10<sup>4</sup>, and 5.89·10<sup>7</sup> cm<sup>-3</sup>; 60%: 3.66·10<sup>6</sup>,  
 363 6.01·10<sup>4</sup> and 1.23·10<sup>8</sup> cm<sup>-3</sup>; and 80%: 5.17·10<sup>6</sup>, 1.32·10<sup>5</sup>, and 2.15·10<sup>8</sup> cm<sup>-3</sup>.

365 Fig. 6a shows the number size distributions of small ions grouped by percentiles of neutral sulfuric  
 366 acid, sulfuric acid dimer and total oxidized organic molecule (OOM) concentration in Beijing. We  
 367 can see that, especially compared to results already for Hyytiälä, the differences in the size

368 distributions with respect to different values of sulfuric acid or OOMs are small for ~~both~~-either  
369 polarities. The concentration of negative ions below approx. 1.2 nm slightly decreases with  
370 increasing sulfuric acid (Fig. 6a, i) and sulfuric acid dimer (Fig. 6a, ii) concentration, while the  
371 concentrations above approx. 1.2 nm increase, indicating a weak but positive relationship between  
372 the sulfuric acid and the negative small ion growth. Close to 2.0 nm, where the increase is the  
373 highest, the concentration of negative ions is higher by around a factor of two when sulfuric acid  
374 concentration is in the 80-100% percentile compared to when it is in the 0-20% percentile (Fig. 6a,  
375 i). For both polarities, the concentrations below approx. 1.75 nm appear higher when the total OOM  
376 concentration is in the 80-100% percentile compared to other times (Fig. 6a, iii and vi). However,  
377 the concentrations close to 2.0 nm are not simultaneously higher, indicating that despite the  
378 increased concentration of small ions, a larger number of them~~more of them are~~ is not growing into  
379 intermediate ions.

380 Fig. 6b shows the scatter plots of  $d_{\text{mean}}$  and sulfuric acid, sulfuric acid dimer and total OOM  
381 concentrations. Weak positive correlation is seen, and the Spearman correlation coefficients ( $r_s$ ) are  
382 between 0.08 and 0.25. The differences in the values of  $d_{\text{mean}}$  are small. The relationship between the  
383 small ion size distribution or  $d_{\text{mean}}$  and low volatility vapor concentrations in Beijing appears weaker  
384 and much less clear compared to Hyytiälä. ~~Due to the high concentration of both low volatility~~  
385 ~~vapors and large particles, the dynamics of small ions in a megacity such as Beijing are different~~  
386 ~~than in a rural site such as Hyytiälä.~~

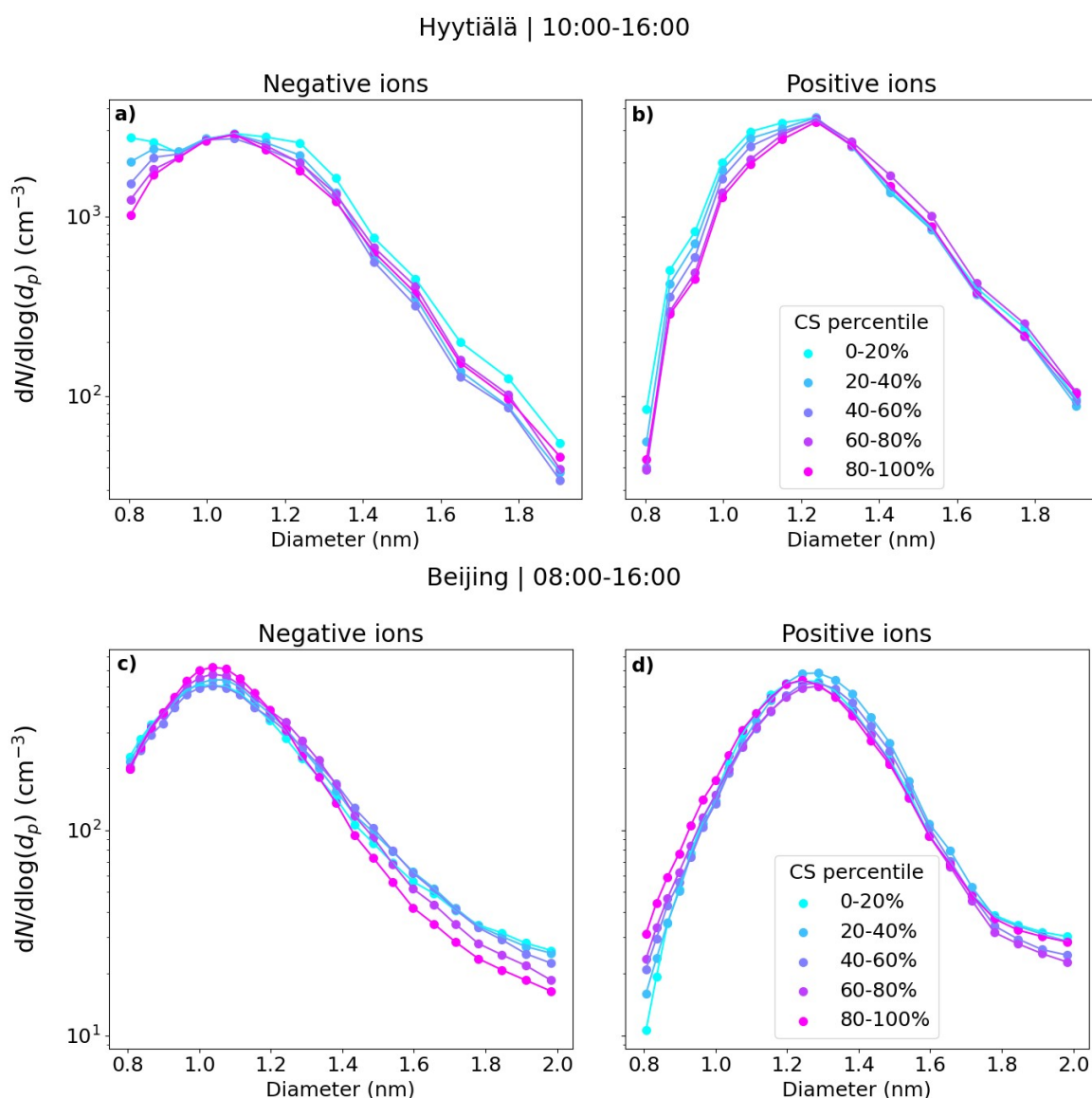
### 387 **3.4 Impact of coagulation scavenging on the small ion size distribution**

388 Fig. 7 shows the median small ion number size distributions in Hyytiälä and Beijing corresponding  
389 to the respective percentiles of condensation sink (CS). We see that the changes in the small ion size  
390 distribution with respect to changing CS are relatively small. In Hyytiälä (Fig. 7a, b), the  
391 concentration of small ions, especially that of the smallest in diameter, decreases slightly with  
392 increasing CS. The sink is relatively low in Hyytiälä, and therefore this result is not unexpected.

393 Based on Fig. A1, which shows the approximate values of the different terms in Eq. 2, we would  
394 expect CoagS to have a much stronger impact on the small ion dynamics in Beijing than in  
395 Hyytiälä. The impact should be most clear for the smallest sizes. Surprisingly, this was not  
396 observed. Fig. 7c shows that in Beijing, the negative small ion size distribution ~~below approx. 1.3~~  
397 nm stays unchanged and the concentrations above decrease with an increasing CS. The larger  
398 positive small ion concentrations (Fig. 7d) also seem to slightly decrease with increasing sink,  
399 while the concentrations of the small ions close to 0.8 nm actually increase. Fig. A2a also shows  
400 that the total sub-2 nm concentration barely changes with changing CS. These results suggest that  
401 there could be a source of unknown nature for small ion cluster formation that is higher when CS is  
402 high, which would compensate for the increased coagulation scavenging of the ions.

403 Fig. A2d-f show the concentrations of the different low volatility vapors as a function of CS. We see  
404 that the concentration of sulfuric acid (Fig. A2d) and sulfuric acid dimers (Fig. A2e) decreases with  
405 increasing sink, as expected. However, the concentration of OOMs (Fig. A2f) increases with  
406 increasing sink. While this is purely speculation, if organic compounds are forming small ion  
407 clusters when the sink is higher, the weak apparent impact of CS on the small ion size distribution  
408 could be explained. Alternative potential explanation could be if there is a positive correlation

409 between CS and the concentration of bases, which stabilize the small clusters. Regardless, the  
 410 impact of CS on the statistics of the small ion size distribution in Beijing appears very small.



411  
 412 Fig. 7: the median small ion size distributions grouped by the respective percentile of the  
 413 condensation sink (CS) values for Hyytiälä (a,b) and Beijing (c, d). The percentile value limits for  
 414 CS in Hyytiälä are  $1.3 \cdot 10^{-3} \text{ s}^{-1}$ ,  $2.3 \cdot 10^{-3} \text{ s}^{-1}$ ,  $3.5 \cdot 10^{-3} \text{ s}^{-1}$ , and  $5.5 \cdot 10^{-3} \text{ s}^{-1}$ . In Beijing, the percentile  
 415 value limits for CS are  $9.3 \cdot 10^{-3} \text{ s}^{-1}$ ,  $1.9 \cdot 10^{-2} \text{ s}^{-1}$ ,  $3.1 \cdot 10^{-2} \text{ s}^{-1}$ , and  $4.5 \cdot 10^{-2} \text{ s}^{-1}$ .

### 416 **3.54 Correlation of small ion size distribution with sulfuric acid clusters** 417 **and NPF in Hyytiälä**

418 Fig. 87a shows the median number size distribution of negative small ions grouped by percentiles of  
 419 the signals of SA ion clusters  $\text{HSO}_4^-$  (monomer),  $\text{H}_2\text{SO}_4 \cdot \text{HSO}_4^-$  (dimer) and  $(\text{H}_2\text{SO}_4)_2 \cdot \text{HSO}_4^-$  (trimer)  
 420 and their ratios in Hyytiälä. The median distributions are determined from daytime (10:00-16:00)  
 421 values, with clear sky conditions. We observe a clear increase in the number of small ions with  
 422 diameters above approx. 1.2 nm with an increased signal of SA ion monomers (Fig. 8a, i) and  
 423 dimers (Fig. 8a, ii). sThe increase is especially clear for dimers and the dimer to monomer ratio

424 | (Fig. 8a, iv), and the concentration of small ions close 2.0 nm, where the differences are highest, is  
425 | an order of magnitude higher when dimer signal is in the 80-100% percentile compared to when the  
426 | signal is in the 0-20% percentile. These results ~~show indicate~~ that the dimer signal is a strong  
427 | indicator for both the cluster formation and the growth of clusters to larger sizes in Hyttiälä.

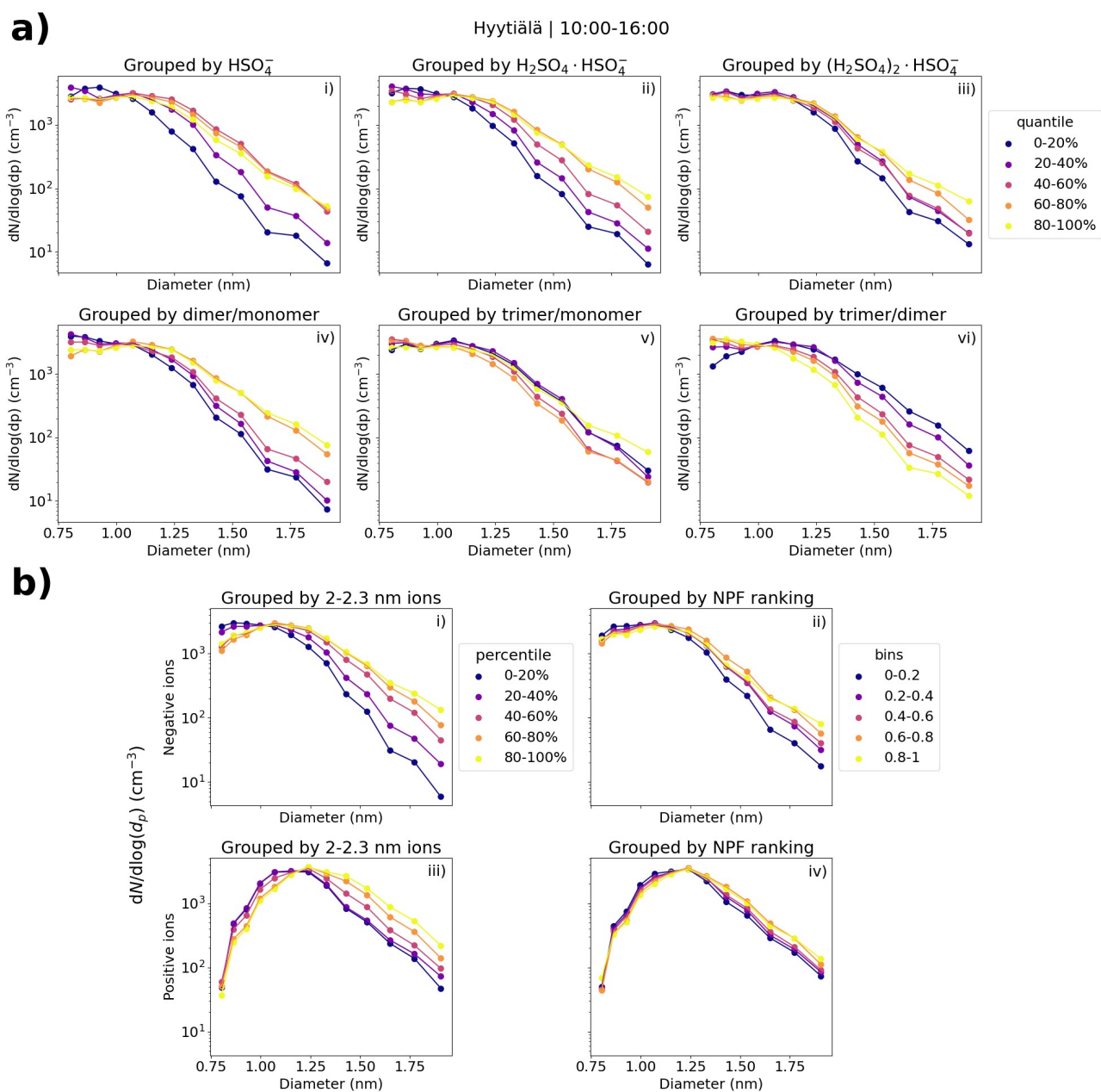
428 | We used the 2.0-2.3 nm ion concentrations and NPF ranking (Aliaga et al., 2023) as proxies for  
429 | conditions that were favorable for cluster formation and growth. Fig. 87b shows the median daytime  
430 | (10:00-16:00) size distributions for both polarities with respect to the percentiles of 2.0-2.3 nm ion  
431 | concentrations and bins of NPF ranking ~~(Aliaga et al., 2023)~~ in Hyttiälä. When the 2.0-2.3 nm ion  
432 | concentration is higher, a clear increase in concentrations is seen above approx. 1.2 nm (Fig. 8b,i  
433 | and iii). The difference in negative small ion concentrations close to 2.0 nm between 80-100% and  
434 | 0-20% is over one order of magnitude (Fig. 8b, i). ~~A high 2.0-2.3 nm ion concentration indicates~~  
435 | ~~intense local-scale cluster formation and NPF (Tuovinen et al., 2024), and we can see from the~~  
436 | ~~small ion size distribution for both polarities how this growth~~The small ion size distribution for both  
437 | ~~polarities shows this growth of small ions up to 2.0 nm, when local-scale intermediate ion formation~~  
438 | ~~is taking place.~~ ~~of small ions up to 2.0 nm is seen in the small ion population as an increase in the~~  
439 | ~~concentrations of larger small ions.~~

440 | Similar observations can be made from the small ion size distributions with respect to the different  
441 | NPF ranking values. However, the differences are smaller than with respect to 2.0-2.3 nm ions, and  
442 | especially for positive small ions such differences are very small (Fig. 8b, iv). There is likely a  
443 | combination of factors at play here. First of all, NPF ranking was determined for total particles  
444 | between 2.5 and 5 nm and there might be differences stemming both from the ranking being less  
445 | sensitive for local NPF, and for 2.0-2.3 nm ion concentrations being more sensitive for ion-induced  
446 | clustering or NPF. In addition, differences between what is observed in the total particles versus  
447 | ions can be caused by variation in the chemical compounds, which take up the available charges  
448 | (Bianchi et al., 2017).

449 | We note that the differences in the number size distribution of positive small ions are once again  
450 | smaller than for negative small ions. Similarly to Sect. 3.2.1, we hypothesize that this is due to the  
451 | size difference between the polarities.

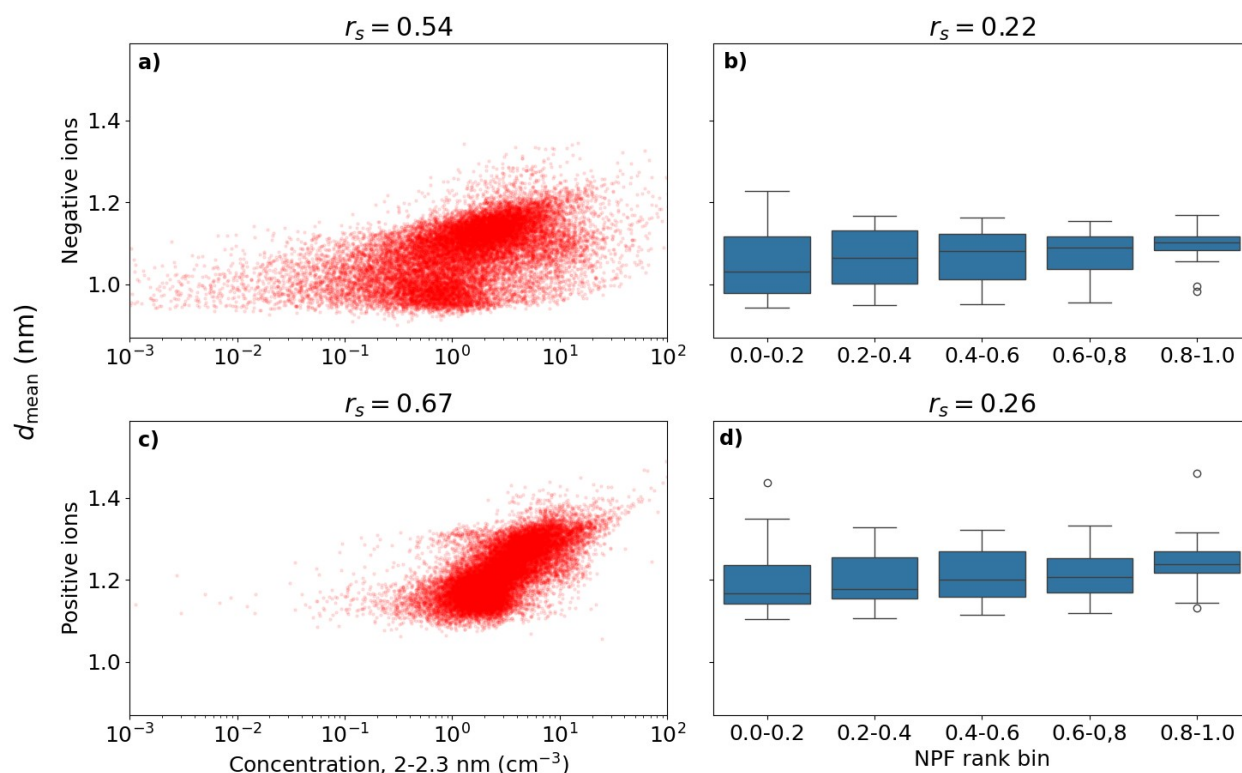
452 | Fig. 98 shows the scatter plot of hourly daytime negative (a) and positive (c) small ion  $d_{\text{mean}}$  and the  
453 | concentration of 2.0-2.3 nm ions. As expected, a strong positive trend is seen between  $d_{\text{mean}}$  and 2.0-  
454 | 2.3 nm ion concentrations. The correlation coefficient is  $r_s = 0.54$  (0.67) for negative (positive) ions.  
455 | Fig. 98 also shows the box plots of  $d_{\text{mean}}$  with NPF ranking, with negative small ions in Fig. 9b and  
456 | positive in 9d. The median of  $d_{\text{mean}}$  increases with increasing NPF ranking, as expected. However,  
457 | the variance for lower rankings is much higher, resulting in overall quite a low correlation between  
458 |  $d_{\text{mean}}$  and NPF ranking,  $r_s =$  for negative (positive small) ions.

459 |

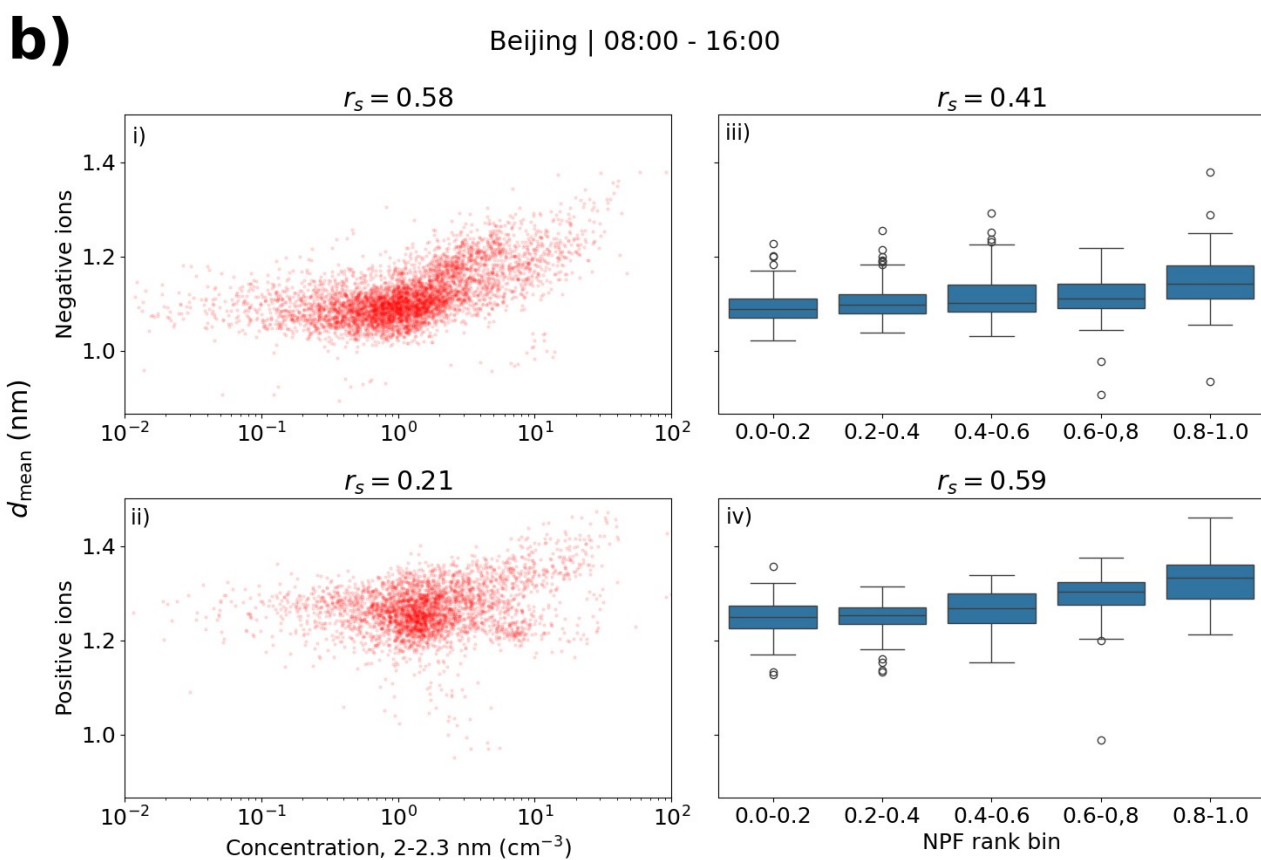
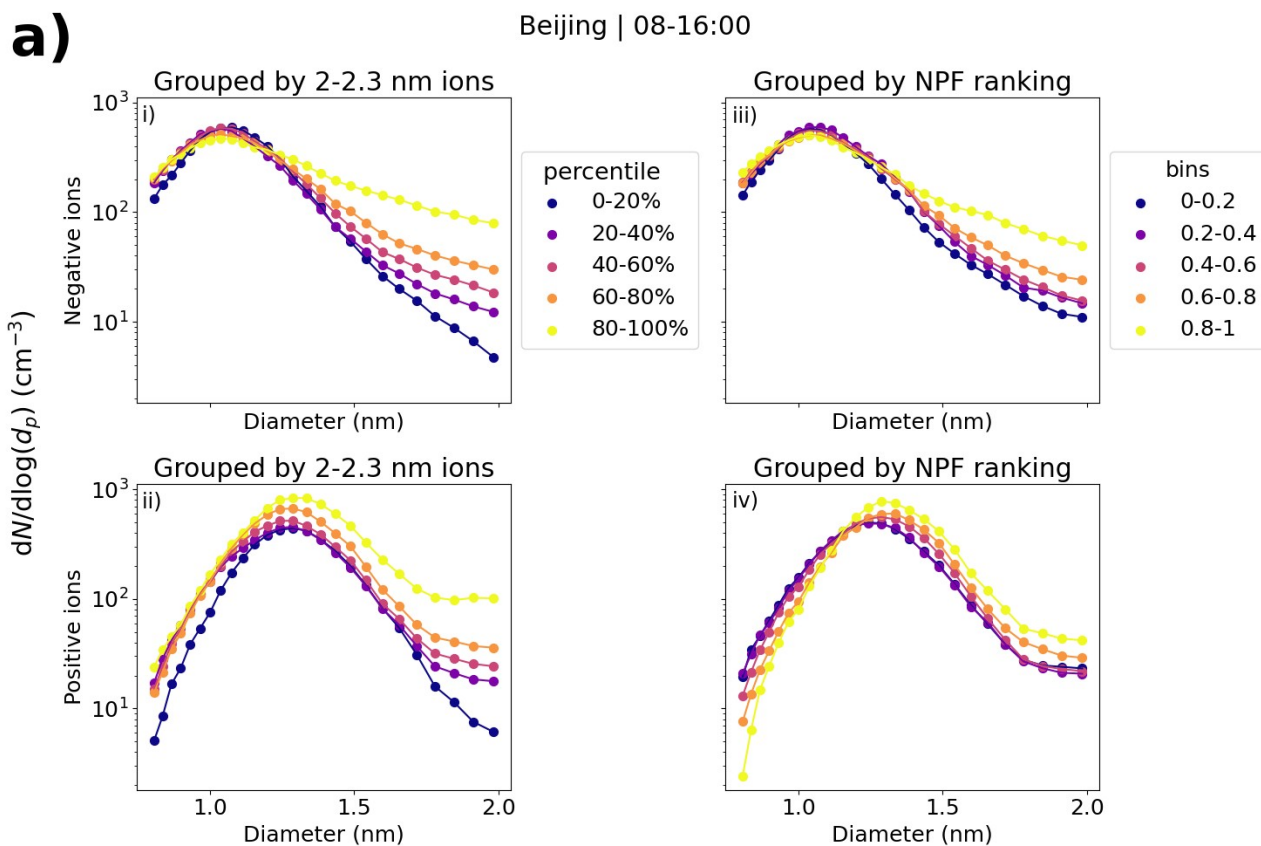


460  
 461 **Fig. 87:** (a) Hyttiälä daytime median negative small ion number size distributions grouped by  
 462 percentile of the signals of  $\text{HSO}_4^-$ ,  $\text{H}_2\text{SO}_4 \cdot \text{HSO}_4^-$  or  $(\text{H}_2\text{SO}_4)_2 \cdot \text{HSO}_4^-$  ions (figures i, ii, iii,  
 463 respectively) and their ratios (figures iv-vi). (b) Daytime median small ion size distributions for  
 464 both polarities grouped by the percentile of 2.0-2.3 nm ion concentrations (figures i, iii)  
 465 of the respective polarity or by NPF ranking (figures ii, iv). The percentile limits for negative (positive)  
 466 2.0-2.3 nm ion concentrations are 20%: 0.48 (1.75)  $\text{cm}^{-3}$ , 40%: 1.01 (2.34)  $\text{cm}^{-3}$ , 60%: 1.94 (3.49)  
 467  $\text{cm}^{-3}$ , and 80%: 3.39 (5.35)  $\text{cm}^{-3}$ .

468  
 469



470  
 471 **Fig. 98:** Hourly daytime negative (a,b) and positive (c, d) small ion diameter versus concentration  
 472 of 2.0-2.3 nm ions of respective polarity (a, c) or NPF ranking (b, c) in Hyytiälä. Correlation  
 473 coefficients ( $r_s$ ) are also shown. The middle line of the box plots for  $d_{\text{mean}}$  and NPF rank are the  
 474 median values, while the boxes show the 25% and 75% percentiles and the lines the 10% and 90%  
 475 percentiles.  
 476  
 477



481 **Fig. 109:** (a) Median negative and positive small ion number size distributions in Beijing grouped  
482 by percentiles of 2.0-2.3 nm ion concentrations ~~(of respective polarity) or by NPF ranking.~~ (b).  
483 Scatter plots of mean diameter and 2.0-2.3 nm ion concentrations (of respective polarity) or NPF  
484 ranking. Figures i-ii are for negative polarity and iii-iv for positive. Values are for daytime (08:00-  
485 16:00). The percentile limits of 2.0-2.3 nm concentration for negative (positive) ions are 20%: 0.51  
486 (0.85)  $\text{cm}^{-3}$ , 40%: 0.92 (1.27)  $\text{cm}^{-3}$ , 60%: 1.33 (1.72)  $\text{cm}^{-3}$ , and 80%: 2.47 (3.22)  $\text{cm}^{-3}$ .

487  
488 Fig. 109a shows the small ion size distributions with respect to the concentration of 2.0-2.3 nm ions  
489 or NPF ranking in Beijing. Negative ions are in Figures i-ii and positive in Figures iii-iv. For both  
490 polarities, clear differences are seen in the distributions depending on the percentile of the 2.0-2.3  
491 nm ion concentration. When the 2.0-2.3 nm ion concentrations are higher, the concentration of  
492 negative (positive) small ions above approx. 1.0 (1.3) nm is increased. Relative to the  
493 concentrations, the differences are largest close to 2.0 nm. Comparing the 0-20% and 80-100%  
494 percentiles, the difference in concentrations is around one order of magnitude when the diameter is  
495 approaching 2.0 nm, comparable to what was observed in Hyytiälä. Similar observations are seen  
496 with respect to NPF ranking, although to a lesser extent. For negative small ions (Fig. 10a, ii), the  
497 concentration at around 2.0 nm is four to five times higher when the NPF ranking is above 0.80  
498 compared to when it is below 0.20. For positive ions, the concentration is less than two times higher  
499 (Fig. 10a, iv).

500  
501 When looking at the small ion distributions in Beijing for different 2.0-2.3 nm ion concentrations or  
502 NPF ranking, unlike for low-volatility vapor concentrations, we are able to see the ~~impact of~~ growth  
503 of small ions to intermediate ions in the size distribution. These results show that the growth of  
504 small ions to larger diameters in Beijing is not limited by the availability of sulfuric acid or oxidized  
505 organic vapors, unlike in Hyytiälä. In addition, based on our analysis it does not appear to be  
506 strongly limited by CS either. This is supported by the relatively weak correlation between CS and  
507 the NPF ranking or 2.0-2.3 nm ions (Fig. A2b,c). Therefore, we speculate that the small ion growth  
508 could be limited more by the availability of bases. However, due to the lack of long-term base  
509 concentration data, this question remains unanswered. In Beijing, CoagS is crucial in determining  
510 whether the growing clusters will survive to larger sizes or not, and therefore, even if the  
511 concentrations of precursors are high, growth might be negligible. A high 2.0-2.3 nm ion  
512 concentration or NPF rank means that a considerable number of clusters are able to grow without  
513 being scavenged by pre-existing larger particles.

514  
515 Fig. 109b shows the scatter plots of  $d_{\text{mean}}$  and 2.0-2.3 nm ion concentration and the box plots of  $d_{\text{mean}}$   
516 and NPF ranking. The correlation coefficients for negative ions are as expected,  $r_s = 0.58$  and  $r_s =$   
517  $0.41$  between  $d_{\text{mean}}$  and 2.0-2.3 nm ion concentration or NPF ranking, respectively. For positive ions,  
518 the correlation coefficient between  $d_{\text{mean}}$  and NPF ranking is  $r_s = 0.59$ , while it is only 0.21 between  
519  $d_{\text{mean}}$  and 2.0-2.3 nm ion concentration. From Fig. 10a we see that the concentrations of positive  
520 small ions below 1.0 nm also increase to some extent with increasing 2.0-2.3 nm ion concentration,  
521 which likely impacts the values of  $d_{\text{mean}}$ , resulting in a relatively poor overall correlation.

522  
523 Notably, the differences in size distributions with respect to NPF ranking are clearer and the  
524 correlation between  $d_{\text{mean}}$  and the ranking is stronger in Beijing than in Hyytiälä for both polarities.  
525 One of the ~~The~~ explaining factors could be the fact that intense NPF in Beijing is more common  
526 than in Hyytiälä (e.g., Dada et al., 2017; Deng et al., 2020), impacting the statistics of the ranking,  
527 and. Another possibility is that local clustering events, where ions or particles grow close to 2.0  
528 nm but not much further, could be more common in Hyytiälä. Overall, our results show that  
529 compared to a rural boreal forest site like Hyytiälä, the dynamics of sub-2 nm ions in a polluted  
530 megacity like Beijing are different.

### 532 | 3.76 Case studies

533 Next, some case studies into the development of negative small ion size distributions, and other  
 534 investigated variables, are presented for Hyytiälä and Beijing. These cases show that we are able to  
 535 observe the cluster growth, driven by daytime NPF or evening clustering, from the ion number size  
 536 distributions of individual days and not only from the statistics of the size distributions. Based on  
 537 the analysis presented in this study, the behavior of negative and positive small ion populations is  
 538 mostly similar, and therefore, for simplicity, we have limited the analysis here to negative polarity.

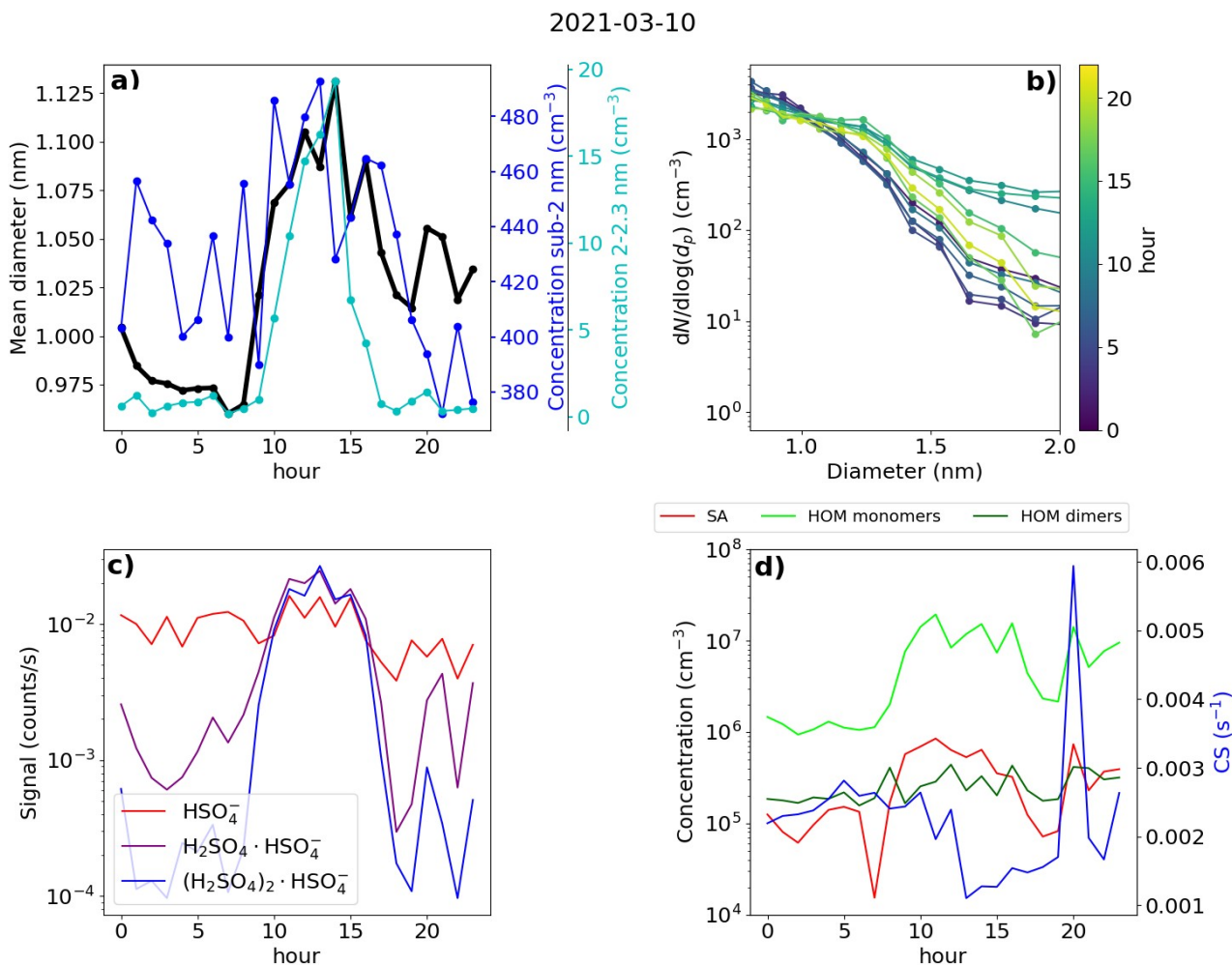
#### 539 | 3.76.1 Hyytiälä case 1 – an early spring day with NPF

540 First of the investigated days was 10<sup>th</sup> of March, in 2021 and is presented in Fig. 110. During this  
 541 day, a strong NPF event was observed with clear growth observed both in the total particle and ion  
 542 number size distribution (see Fig. A34). In the morning, a strong increase in the SA ion dimer and  
 543 trimer signals was detected after 07:00 (Fig. 110c), which occurred simultaneously with an increase  
 544 in the concentration of neutral sulfuric acid. Shortly after, at around 08:00, neutral HOM monomer  
 545 concentration started to increase (Fig. 110d). A strong increase in the concentration of 2.0-2.3 nm  
 546 negative ions was observed after 09:00, indicating intense NPF on a local-scale (Fig. 110a).  
 547 Approximately one hour before an increase in the concentration of 2.0-2.3 nm ions was first  
 548 observed, the small ion  $d_{\text{mean}}$  started to increase from below 1.0 nm (Fig. 11a), showing that growth  
 549 of clusters in the small ion population to larger sizes had begun. We can also see this from the  
 550 negative ion number size distributions (0.8-2.0 nm; Fig. 110b): in the early hours of the day, the  
 551 concentrations of the smallest ions are at their highest while the concentration of ions above approx.  
 552 1.1 nm are at their lowest. Throughout the morning hours, we can see that the concentration of ions  
 553 above approx. 1.1 nm increases and in the afternoon, around 14:00, the concentration of ions close  
 554 to 2.0 nm is over a order of magnitude higher than during the night before. At around 14:00, the  
 555 concentration of 2.0-2.3 nm ions and small ion  $d_{\text{mean}}$  also reach their peaks. At the same time, CS is  
 556 at its lowest (Fig. 11d). Then, the concentrations of larger small ions, 2.0-2.3 nm and SA ion  
 557 clusters starts to decrease, alongside with the concentration of HOM monomers.

558 We also took a look at the diameter specific concentrations in a smaller time frame (Fig. A64),  
 559 which clearly shows how clear increase concentrations is observed for the diameters above 1.2 nm.  
 560 A time delay between the increasing concentration of larger ions and smaller ions was seen,  
 561 showing the growth of ions between 1.2 to 2.0 nm. Using the appearance time method (Lehtipalo et  
 562 al., 2014), GR between 1.24 to 2.05 nm was estimated: GR = 0.40 nm/h. This value is somewhat  
 563 lower than typical GRs reported in Hyytiälä (Hirsikko et al., 2005; Yli-Juuti et al., 2011), as  
 564 expected due to the small size of the considered ions. Regardless, it shows that the growth of ions  
 565 below 2.0 nm is non-negligible on this particular day. We note that this GR, or the ones presented  
 566 for Hyytiälä Case 2 and Beijing Case, is not a representative of the whole range of GRs for similar  
 567 cases in the same location, and that there can be considerable variability.

568 This day clearly shows how the sulfuric acid and HOM driven particle formation is seen as the  
 569 growth of the small ions to larger diameters. With the ion size distribution data, we have been able  
 570 to get insight on when the cluster growth starts and how it progresses throughout this day. the  
 571 connection between sulfuric acid and HOMs with particle formation, and illustrates how the small

572 | ion number size distribution changes as the ions grow from close to 1 nm in diameter to above 2  
 573 | nm.  
 574 |



575  
 576 | **Fig. 110:** Data from Hyytiälä, 10<sup>th</sup> of March, 2021. (a) Hourly mean diameter of negative small ions  
 577 | (0.8-2.0 nm), total concentration of small ions, and concentration of 2.0-2.3 nm negative ions. (b)  
 578 | Two-hour median number size distribution of negative small ions. (c) Hourly signals of HSO<sub>4</sub><sup>-</sup>,  
 579 | H<sub>2</sub>SO<sub>4</sub>·HSO<sub>4</sub><sup>-</sup> and (H<sub>2</sub>SO<sub>4</sub>)<sub>2</sub>·HSO<sub>4</sub><sup>-</sup> ions. (d) Hourly median concentrations of neutral sulfuric acid  
 580 | (SA) and highly oxidized molecule (HOM) monomers and dimers, and the condensation sink (CS).  
 581 |

### 582 | 3.76.2 Hyytiälä Case 2 – a spring day with strong evening clustering

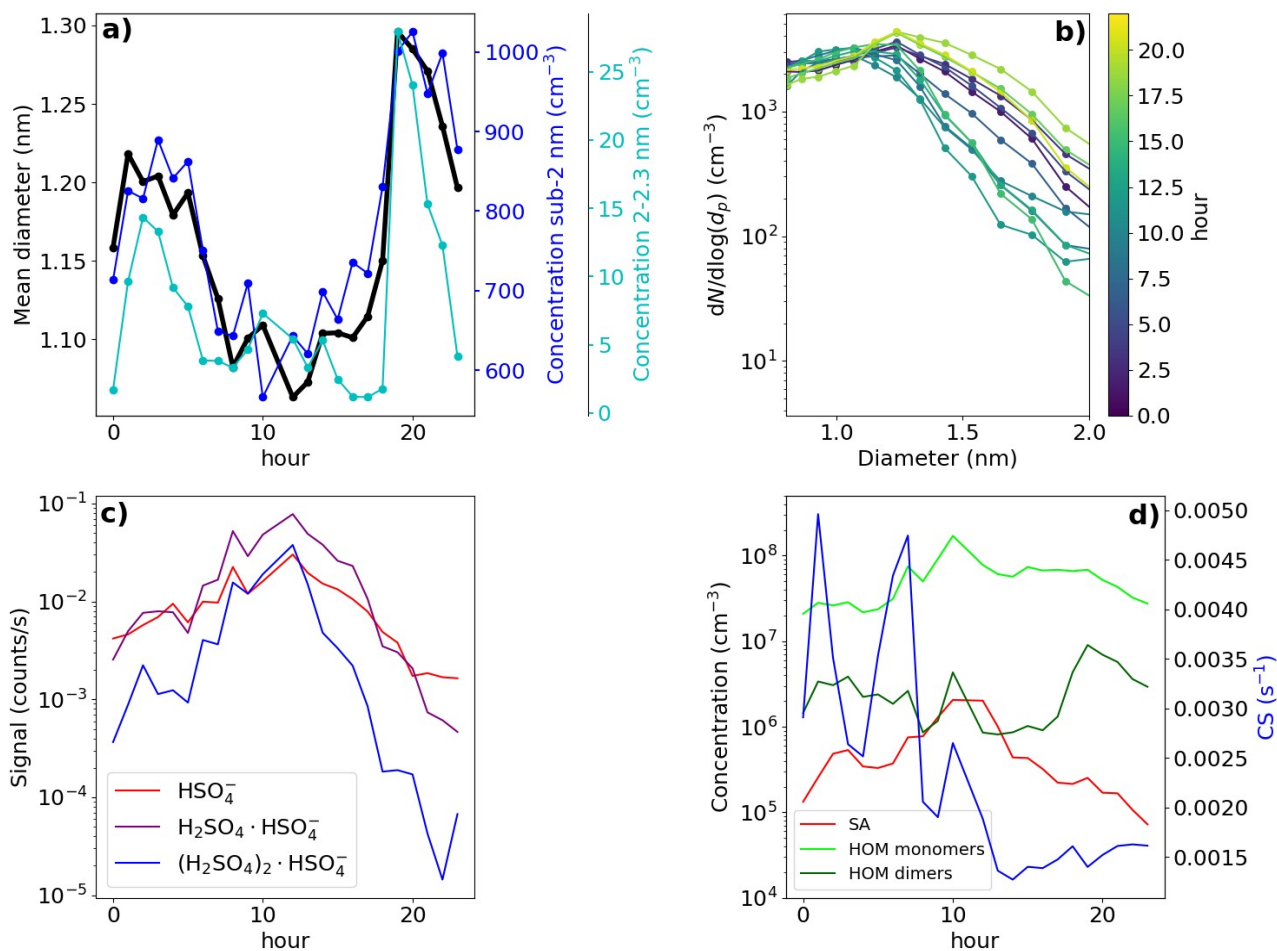
583 | The second of the chosen days for Hyytiälä is 19<sup>th</sup> of April, 2021 (Fig. 121). The NPF ranking of  
 584 | this day was high, over 0.9, however the growth in the negative ion and total particle mode was  
 585 | discontinuous with the clearest growth observed above 5.0 nm, suggesting that the fraction of  
 586 | growing locally formed neutral clusters or ions was low (Fig. A42). However, strong evening ion  
 587 | cluster formation was observed on this day. Therefore, Case 2 illustrates both the ~~probable~~  
 588 | contribution of organic vapors to initiate the growth of larger particles and the evening ion cluster  
 589 | formation attributable to HOM dimers (Mazon et al., 2016).

590 | Starting from the early hours of the day, the signals of SA ions and neutral SA concentration  
 591 | increase (Fig. 121c and 121d), reaching their maxima around 13:00 in the early afternoon.

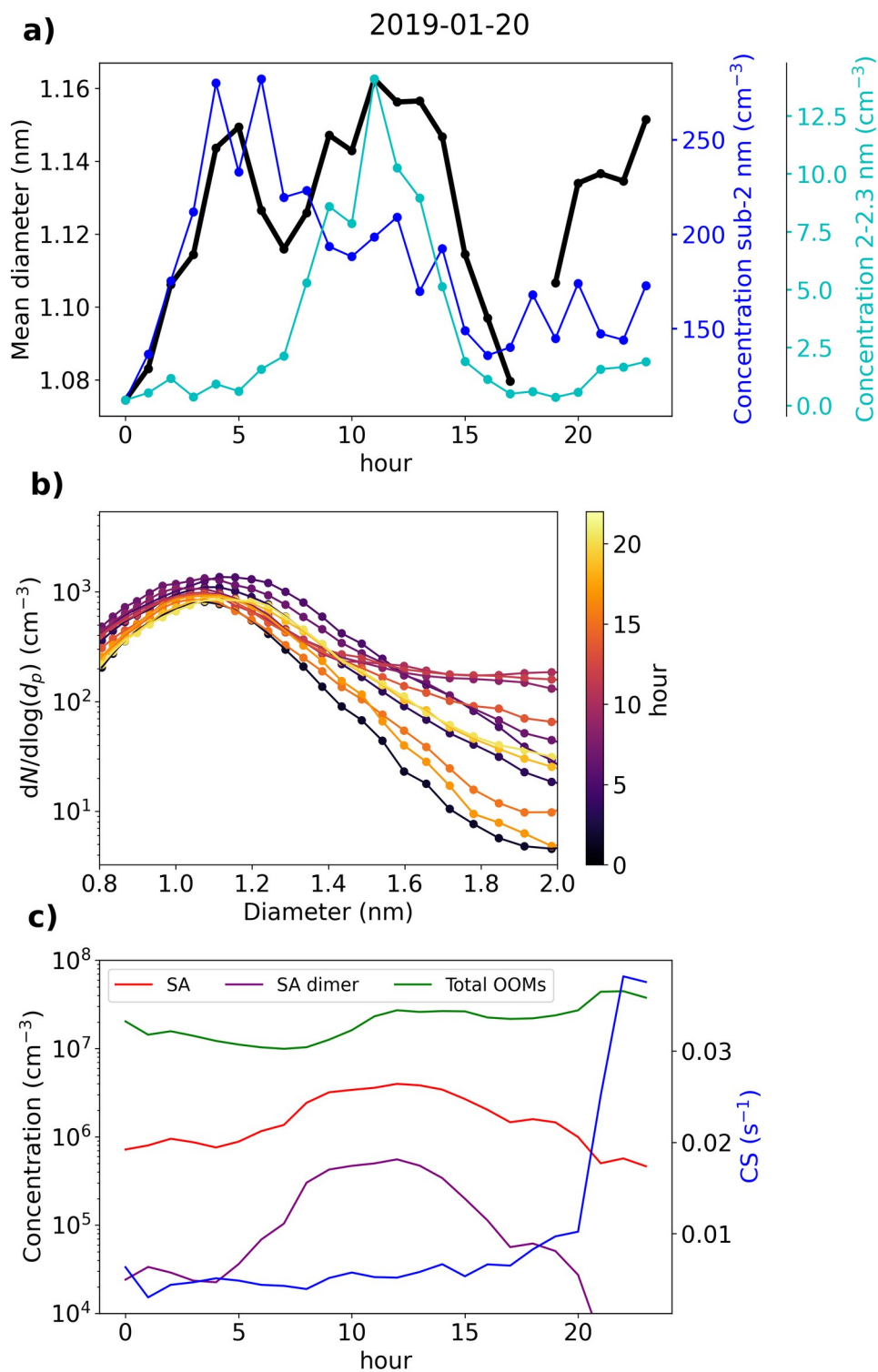
592 Compared to Hyytiälä Case 1, the signal from trimers is lower in relation to the signal from  
593 monomer and dimer. At the same time, CS decreases (Fig. 12d). From the negative ion number size  
594 distributions (Fig. 12b), we see that the concentration of negative ions below approx. 1.2 nm  
595 increases and the concentration of small ions above approx. 1.2 nm strongly decreases starting from  
596 the early hours of the day until afternoon. This is reflected in the value of  $d_{\text{mean}}$ , which decreases  
597 from over 1.2 nm to below 1.1 nm (Fig. 12a). The concentration of 2.0-2.3 nm negative ions  
598 decreases until 08:00 in the morning, after which it increases briefly before decreasing again (Fig.  
599 12a). The small ion total concentration also strongly decreases from over 800 cm<sup>-3</sup> to 600 cm<sup>-3</sup>  
600 (Fig. 12a). Unlike in Case 1, on this day, the growth of small ions during daytime is negligible and  
601 an increased fraction of the available charge is taken up by small, below 1.2 nm ions, many of  
602 which are likely composed of sulfuric acid monomers or dimers. This explains the behavior of the  
603 ion size distributions,  $d_{\text{mean}}$  and the total small ion concentration.

604 After 14:00 in the afternoon, the concentration of neutral HOM dimers starts to increase, and  
605 reaches a peak at around 19:00 (Fig. 12d). Compared to Case 1, the HOM dimer concentration is  
606 over one order of magnitude higher. Notably, at the same time as the HOM dimer concentration  
607 starts increase, clear growth of total particles above 5.0 nm is observed (Fig. A42). Concentration of  
608 small ions larger than approx. 1.2 nm (Fig. 12b) and 2.0-2.3 nm ion concentration (Fig. 12a)  
609 strongly increase. Small ion  $d_{\text{mean}}$  increases from approx. 1.1 nm to 1.3 nm, while the total negative  
610 small ion concentration increases from around 600 cm<sup>-3</sup> to 1000 cm<sup>-3</sup>. The negative ion GR between  
611 1.43 to 2.05 nm was estimated to be 1.28 nm/h (Fig. A64), which is over twice as high as the GR  
612 estimated for Case 1, likely due to the high concentration of lower volatility HOMs driving the  
613 small ion growth during this particular evening.

2021-04-19



614  
 615 | **Fig. 121:** Data from Hyytiälä, 19<sup>th</sup> of April, 2021. (a) Hourly mean diameter of negative small ions  
 616 (0.8-2.0 nm), total concentration of small ions, and concentration of 2.0-2.3 nm negative ions. (b)  
 617 Two-hour median number size distribution of negative small ions. (c) Hourly signals of HSO<sub>4</sub><sup>-</sup>,  
 618 H<sub>2</sub>SO<sub>4</sub>·HSO<sub>4</sub><sup>-</sup> and (H<sub>2</sub>SO<sub>4</sub>)<sub>2</sub>·HSO<sub>4</sub><sup>-</sup> ions. (d) Hourly median concentrations of neutral sulfuric acid  
 619 (SA) and highly oxidized molecule (HOM) monomers and dimers, and the condensation sink (CS).  
 620 |



624 | **Fig. 132:** Data from Beijing, 20<sup>th</sup> of January, 2019. (a) Hourly mean diameter of negative small ions  
 625 (0.8-2.0 nm), total concentration of small ions, and concentration of 2.0-2.3 nm negative ions. (b)  
 626 Two-hour median number size distribution of negative small ions. (c) Hourly median concentrations

627 of neutral sulfuric acid (SA), SA dimer, and total oxidized organic molecules (OOMs), and  
628 condensation sink (CS).

629

630 Fig. 132 presents data from Beijing on 20<sup>th</sup> of January, 2019. This day was characterized by an  
631 intense NPF event, observed both in the ion and the total particle size distribution (Fig. A53). We  
632 see that from 00:00 until 05:00 in the morning, the negative small ion concentrations seem to  
633 increase, which is apparent for the whole sub-2 nm size range (Fig. 132a and 132b).  
634 Simultaneously,  $d_{\text{mean}}$  of the small ions increases (Fig. 13a). The concentration of 2.0-2.3 nm  
635 negative ions stays low (Fig. 132a), indicating that there is no significant growth of small ions to  
636 intermediate ions. CS is similar throughout the night and the early morning. Based on the data  
637 presented here, we hypothesize that the increase in small ion concentration is attributed to a larger  
638 fraction of the ions being detected by the instrument as  $d_{\text{mean}}$  increases. The increase in small ion  
639 concentration could be due to reduction in CS or even meteorological conditions.

640 After 05:00 in the morning, an increase in neutral sulfuric and sulfuric acid dimer concentration is  
641 observed (Fig. 132c). Simultaneously, the concentration of 2.0-2.3 nm ions increases sharply,  
642 indicating the formation of intermediate ions. Two changes in the small ion size distribution are  
643 shown: first, the concentration of small ions below approx. 1.5 nm ions, decreases and second, the  
644 concentration of small ions above that increases. Increasing growth of small ions to larger sizes  
645 causes a shift in their size distribution. Notably, no growth in the surface plots (Fig. A53) is  
646 observed yet, likely due to locality of or insufficient intensity of the ion formation. After 12:00, the  
647 concentrations of small ions larger than approx. 1.5 nm start to decrease, as does the concentration  
648 of 2.0-2.3 nm ions. While the growth of ions and particles at larger diameters continues, the  
649 intensity of the cluster growth decreases.

650 In this case, the negative small ion GR was estimated to be 0.24 nm/h from 1.72 to 2.06 nm (Fig.  
651 A75), which is lower than the values determined for the two Hyytiälä cases and is on the lower  
652 range of values of particle GRs for Beijing (Deng et al., 2020). Another noteworthy observation can  
653 be made from the diameter specific concentrations (Fig. A75): as already seen from the size  
654 distributions and more clearly here, the concentrations of ions up to around 1.5 nm decrease, while  
655 the concentrations above increase at the same time. This implies that the ions, which actually start  
656 to grow to larger sizes are close to 1.5 nm in diameter, though at such a low GR their survival  
657 probability to larger sizes is likely very low (Kulmala et al., 2017).

658 In Sect. 3.3, we saw how in Beijing there does not seem appeared to be ~~no~~-correlation between the  
659 small ion number size distribution and the concentration of sulfuric acid. On this day, the increased  
660 concentrations of sulfuric acid occurred approx. simultaneously with the observed small ion growth.  
661 Previous studies have shown the importance of sulfuric acid in particle formation in Beijing (Yao et  
662 al., 2018; Cai et al., 2021; Yan et al., 2021). As such, it seems likely that the growing small ions  
663 seen on this day are composed of sulfuric acid. However, while sulfuric acid forms these growing  
664 clusters, their growth also requires other ingredients. However, this day shows that despite the poor  
665 overall correlation, on some days there does appear to simultaneously be an increase in sulfuric acid  
666 concentration, and an increase in the growth of small ions.

## 667 4 Conclusions

668 We studied the seasonality of small ion number size distribution and the relationship of the small  
669 ion size distribution with low-volatility organic vapors, sulfuric acid, coagulation sink (CoagS) and  
670 NPF in a rural boreal forest location of Hyytiälä, Finland and an urban megacity location of Beijing,  
671 China. Both analysis of long time series of data and daily case studies were carried out. We found a  
672 clear seasonality of the small ion size distribution in Hyytiälä, where the small ions of both  
673 polarities were the smallest in size during winter and the largest during late spring and summer. In  
674 Beijing, while there were month-to-month variations in the size distribution, but no clear seasonal  
675 pattern was identified, ~~which we note could partly be due to the smaller number of data from~~  
676 Beijing compared to Hyytiälä.

677 We found that in Hyytiälä the small ion size distribution strongly varied with respect to the  
678 concentration of organic, especially highly oxidized organic (HOM) monomer, compounds and that  
679 the concentration of small ions above approx. 1.2 nm increased strongly with increasing HOM  
680 monomer concentration. This was observed more strongly for negative polarity and during the  
681 evening, which was found to be connected to the evening ion cluster formation driven by organics  
682 in Hyytiälä. The small ion size distribution also showed clear increase in the size of the small ions  
683 in Hyytiälä with respect to neutral sulfuric acid and ionized sulfuric acid dimers, associated with  
684 daytime cluster formation and growth. In contrast, there was no clear relationship between the  
685 concentration of either organic vapor or sulfuric acid and the size of the small ions in Beijing. The  
686 reason for this remains to be ~~un~~identified, but we hypothesize that the concentration of bases is the  
687 limiting factor determining if growth of small ions is seen in Beijing. ~~the high scavenging loss rate~~  
688 ~~of ions could suppress or hide the impact of these vapors on the small ion size distribution.~~

689 We found that the small ion size distribution in either location did not change strongly with  
690 changing CoagS. In Hyytiälä, small decrease in the concentration of especially the smallest ions  
691 was seen, as expected. However, despite our expectations, this was not observed in Beijing. The  
692 reason for this remains to be answered in future research.

693 When the concentration of ions in the range 2.0-2.3 nm increased, indicating the occurrence of local  
694 NPF, we observed clear signs of growth in the small ion size distribution. This was seen in both  
695 locations, even in Beijing, where no clear association of small ion size with organic vapor or  
696 sulfuric acid was found. To a lesser extent, an increase in the small ion size was also seen with  
697 respect to NPF rank, a parameter, which characterizes the intensity of NPF. These results support  
698 the conclusion that in Beijing the concentration of sulfuric acid or organic vapor does not determine  
699 whether small ions grow to intermediate ions.

700 Overall, ~~we~~our results have shown in a novel way how the atmospheric cluster formation and  
701 growth processes impact the number size distribution of small ions. ~~We have also shown how the~~  
702 ~~small ion size distribution can be used to observe and get insight into these processes. The sub-2 nm~~  
703 ~~size range is integral for understanding of the first steps of new particle formation and the activation~~  
704 ~~of the clusters to grow into particles. Our results can be applied in research into the dynamics of~~  
705 ~~charged clusters and how they grow from clusters to particles.~~

## 706 **Author contributions**

707 ST analyzed the data and wrote the manuscript. JL was responsible for the ion measurements in  
708 Hyytiälä. CL and NS were responsible for the measurements of low-volatility vapors and ion  
709 clusters. YL was responsible for the measurements in Beijing. MK and VMK conceptualized the  
710 study. All authors contributed to reviewing and editing the manuscript.

## 711 **Code and data availability**

712 The Hyytiälä DMPS dataset can be accessed through the SmartSMEAR data portal at  
713 <https://smear.avaa.csc.fi/>. Other data and the codes used to produce the figures in this paper are  
714 available upon request from the authors.e

## 715 **Competing interests**

716 At least one of the (co-)authors is a member of the editorial board of Aerosol Research. Authors  
717 have no other competing interests to declare.

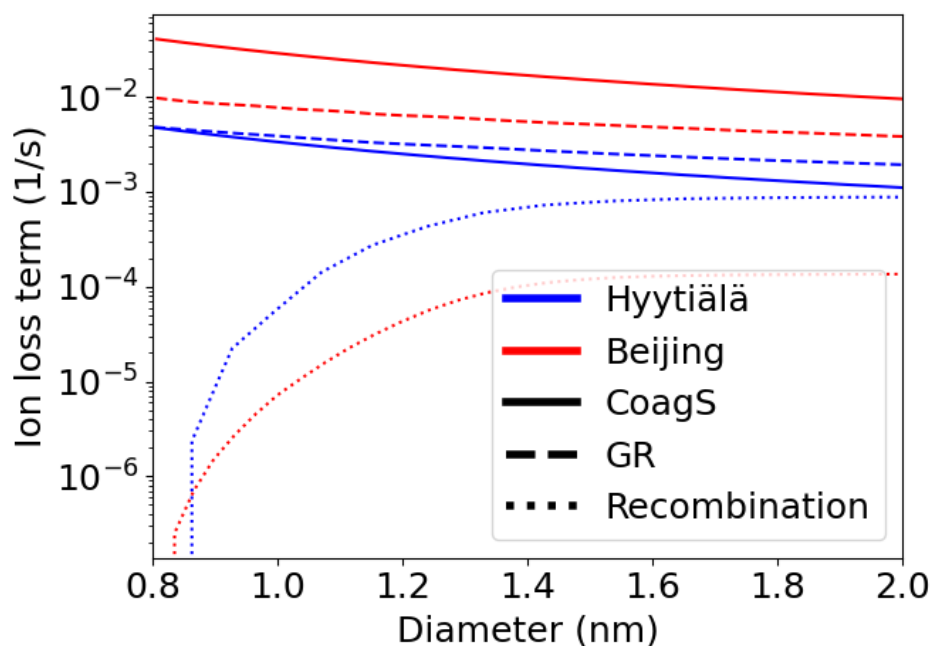
718

## 719 **Acknowledgments**

720

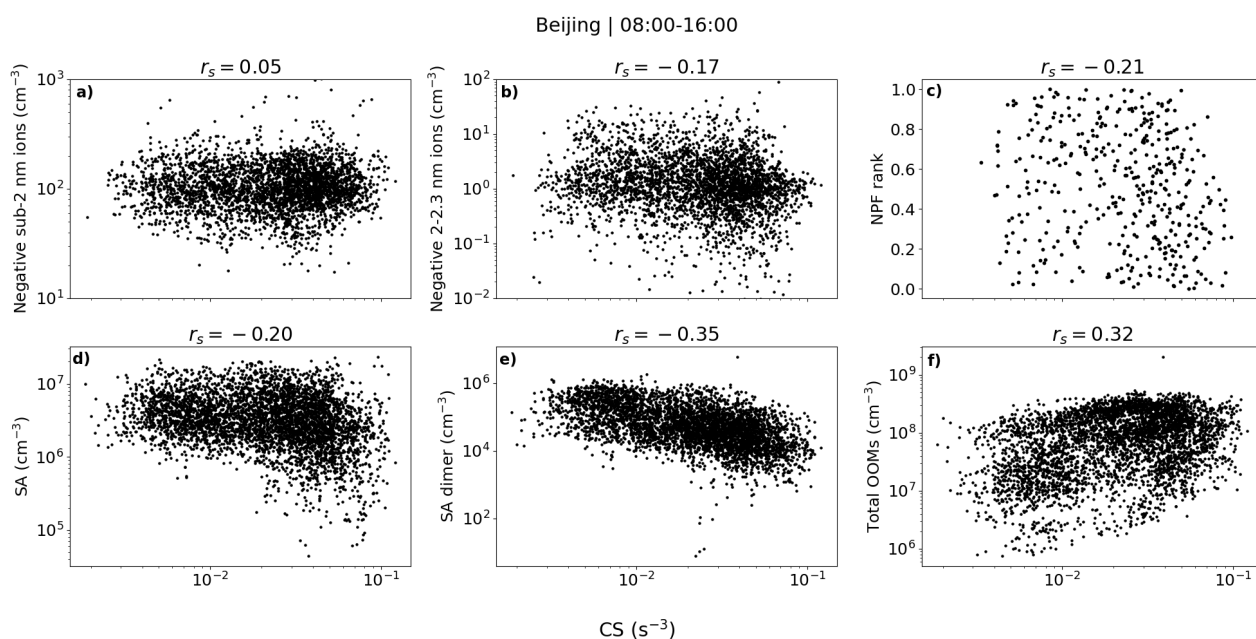
721 This work has been supported by the ACCC Flagship funded by the Academy of Finland grant nos.  
722 337549 (UH) and 337552 (FMI), and the “Gigacity” project funded by the Jenny and Antti Wihuri  
723 Foundation. We acknowledge the SMEAR II and AHL/BUCT technical and scientific staff.

## 724 **Appendix**



725

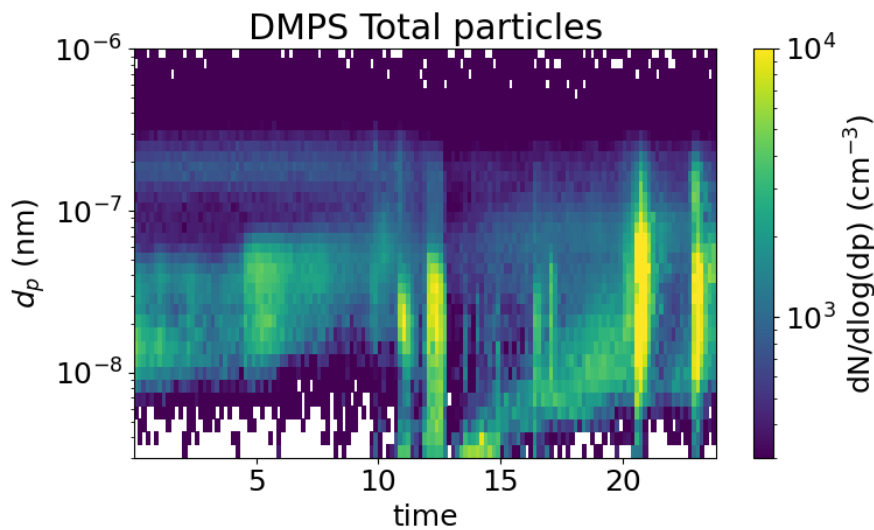
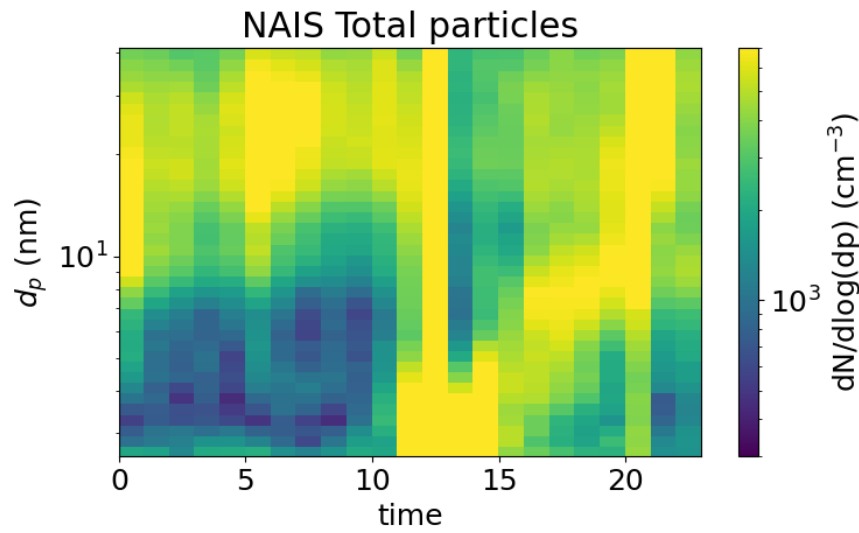
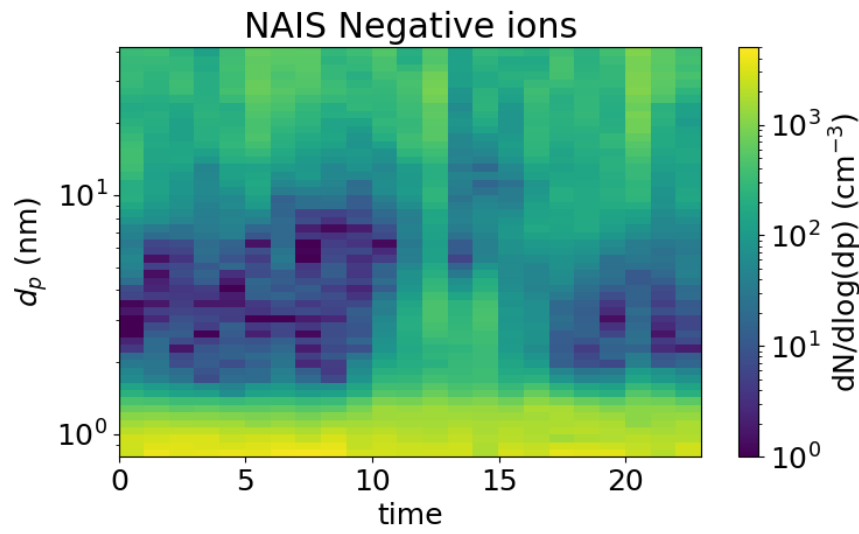
726 **Fig. A1:** A rough approximation of the different loss terms of negative ions as a function of ion  
 727 diameter based on Eq. 2 in both Hyytiälä and Beijing. The concentration of positive ions were based  
 728 on the median number size distributions. GR was assumed to equal 1 nm/h and was assumed to be  
 729 constant with diameter. CoagS was scaled based on the median CS, and assuming that the charge  
 730 enhancement of the sink was by a factor of 2. The median CS were  $CS=2.9 \cdot 10^{-3} \text{ s}^{-1}$  and  $2.5 \cdot 10^{-2} \text{ s}^{-1}$ ,  
 731 for Hyytiälä and Beijing, respectively.



732

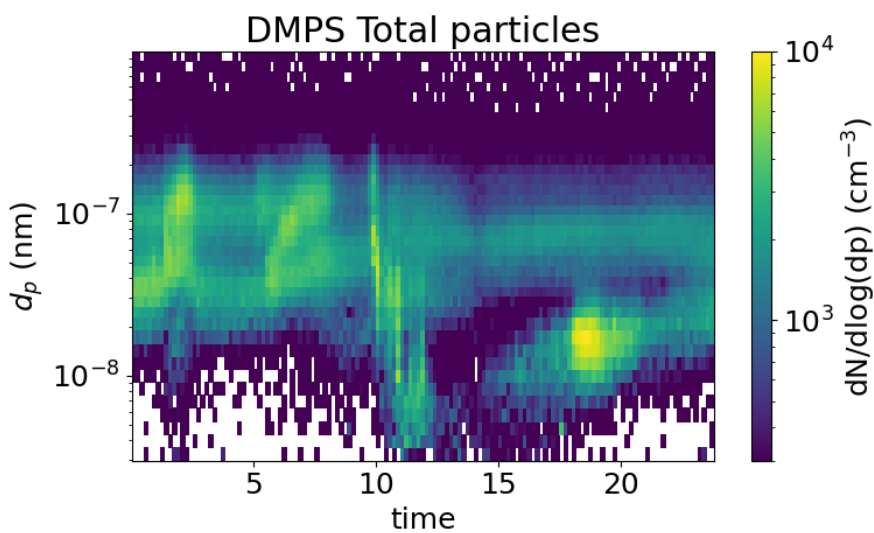
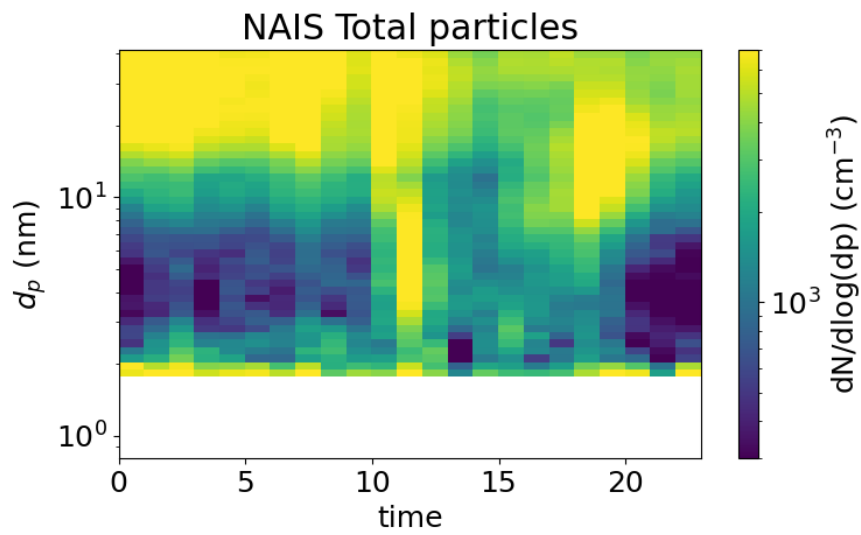
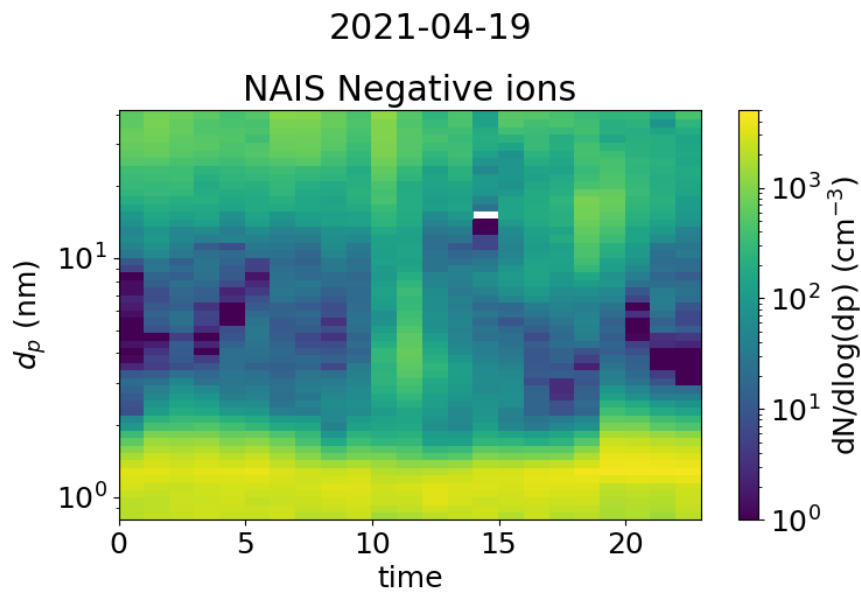
733 **Fig. A2:** The concentrations of negative sub-2 nm (a) and 2.0-2.3 nm (b) ions, NPF ranking values  
 734 (c), and the concentrations of neutral sulfuric acid (SA, d), SA dimer (e), and total oxidized organic  
 735 molecules (OOMs, f) with respect to condensation sink (CS) in Beijing. The values are hourly  
 736 medians, except for c), where NPF ranking is a daily parameter and CS is the daytime median. The  
 737 Spearman correlation coefficients ( $r_s$ ) are also shown.

2021-03-10



738

739 | **Fig. A31:** Surface plots of negative ion number size distribution and total particle number size  
740 distribution measured by NAIS and DMPS in Hyytiälä on 10<sup>th</sup> of March, 2021.

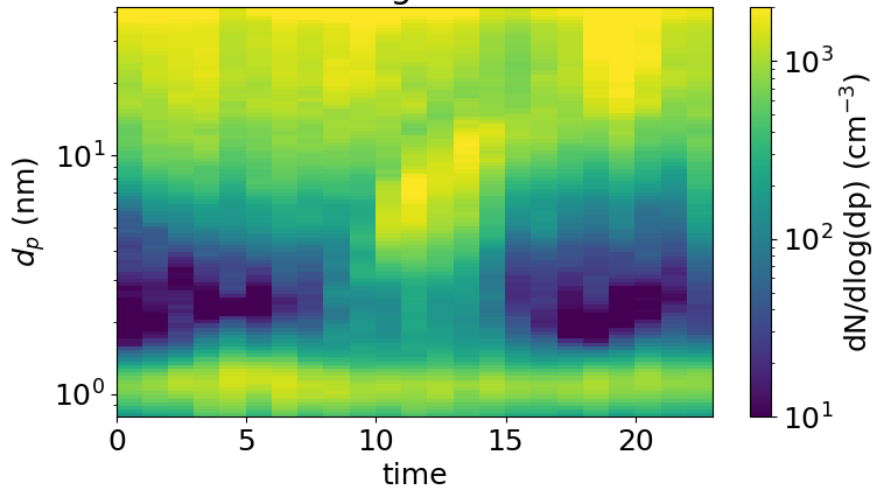


741

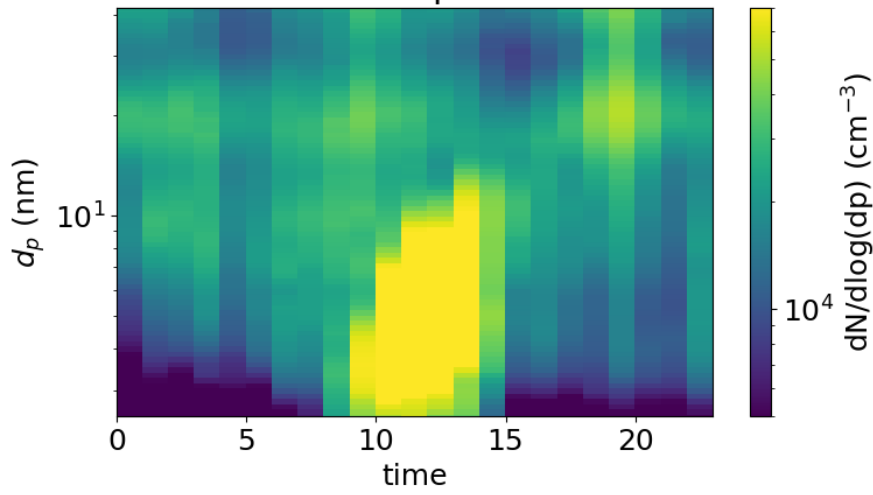
742 | **Fig. A42:** Surface plots of negative ion number size distribution and total particle number size  
 743 distribution measured by NAIS and DMPS in Hyytiälä on 19<sup>th</sup> of April, 2021.

2019-01-20

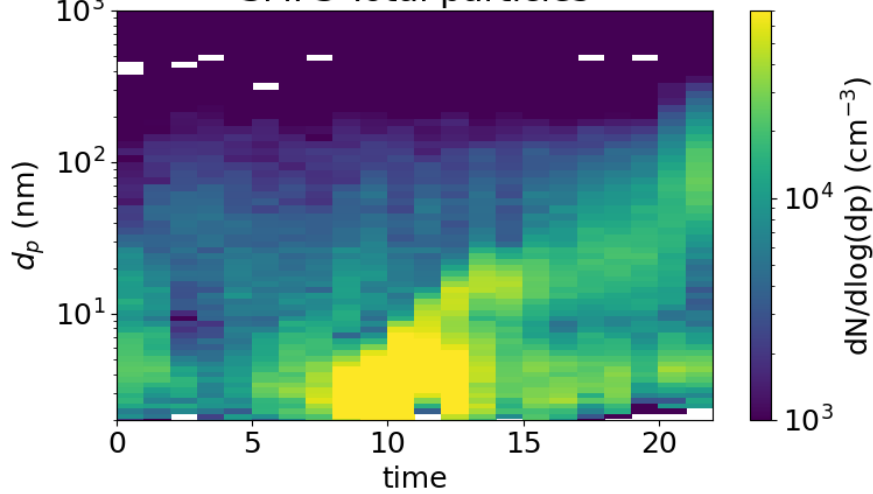
NAIS Negative ions



NAIS Total particles

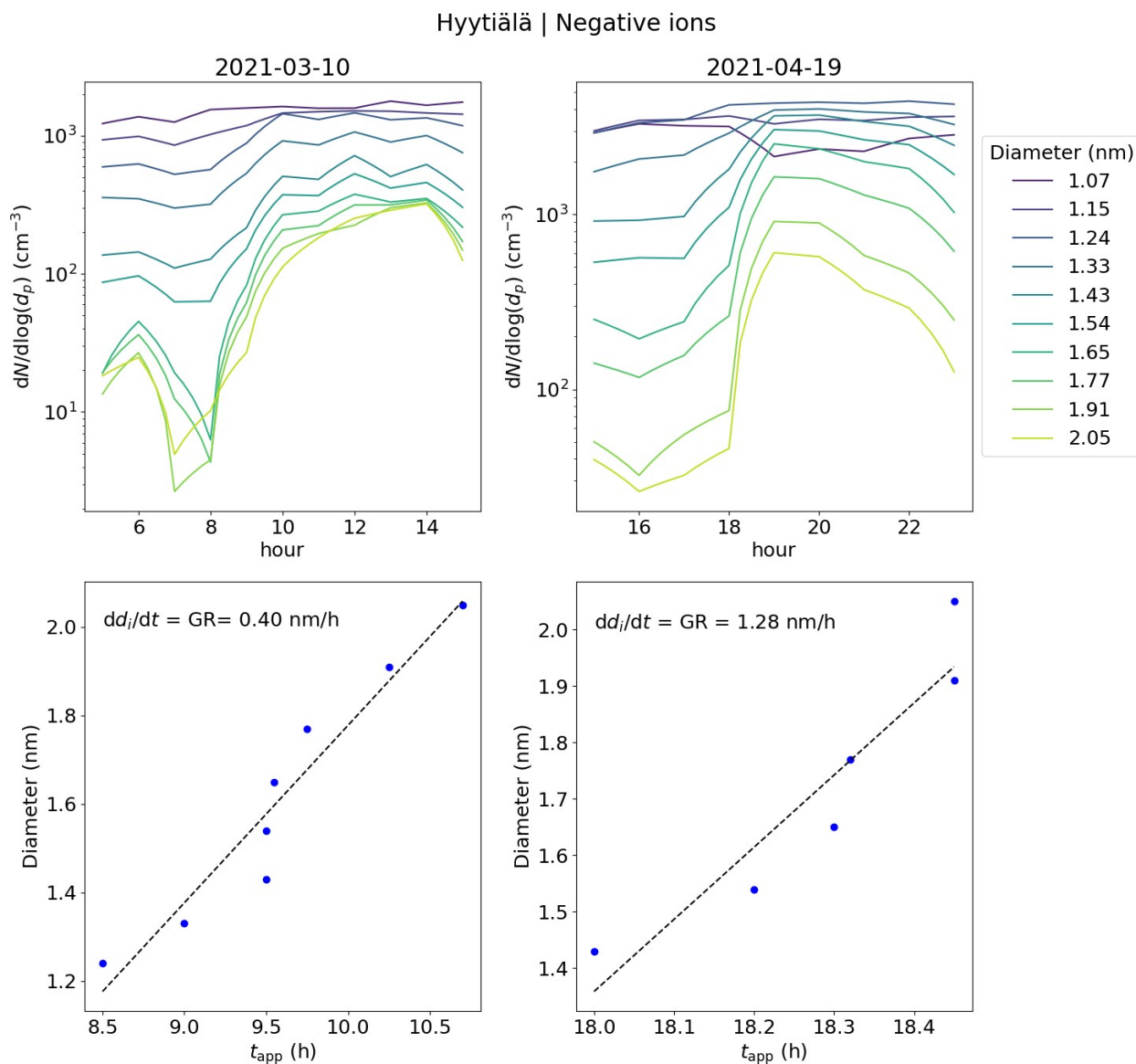


SMPS Total particles



745 | **Fig. A53:** Surface plots of negative ion number size distribution and total particle number size  
 746 distribution measured by NAIS and SMPS (see Liu et al., 2016 for more information) in Beijing on  
 747 20<sup>th</sup> of January, 2019.

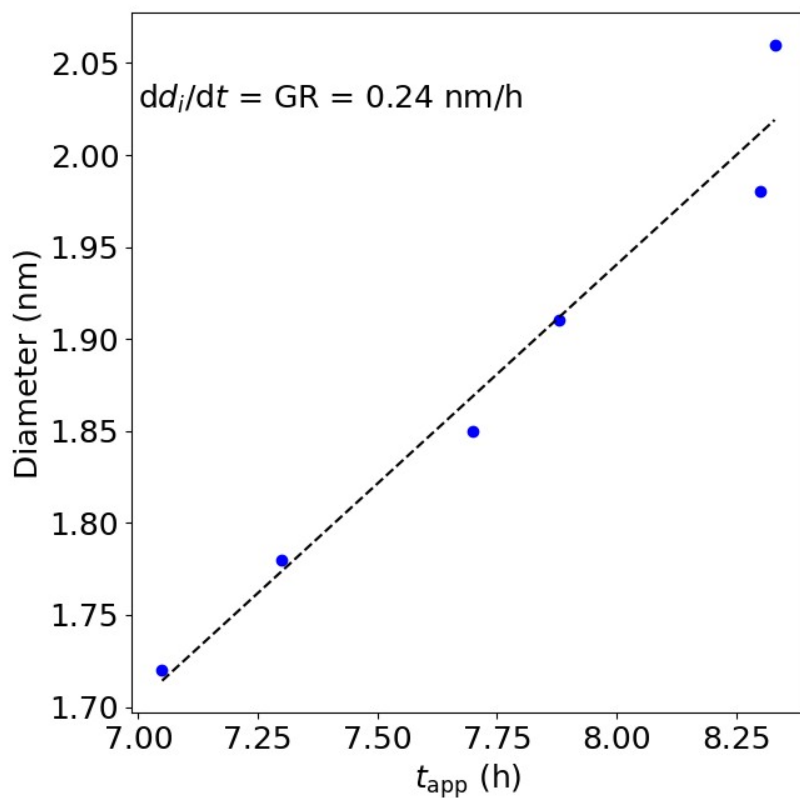
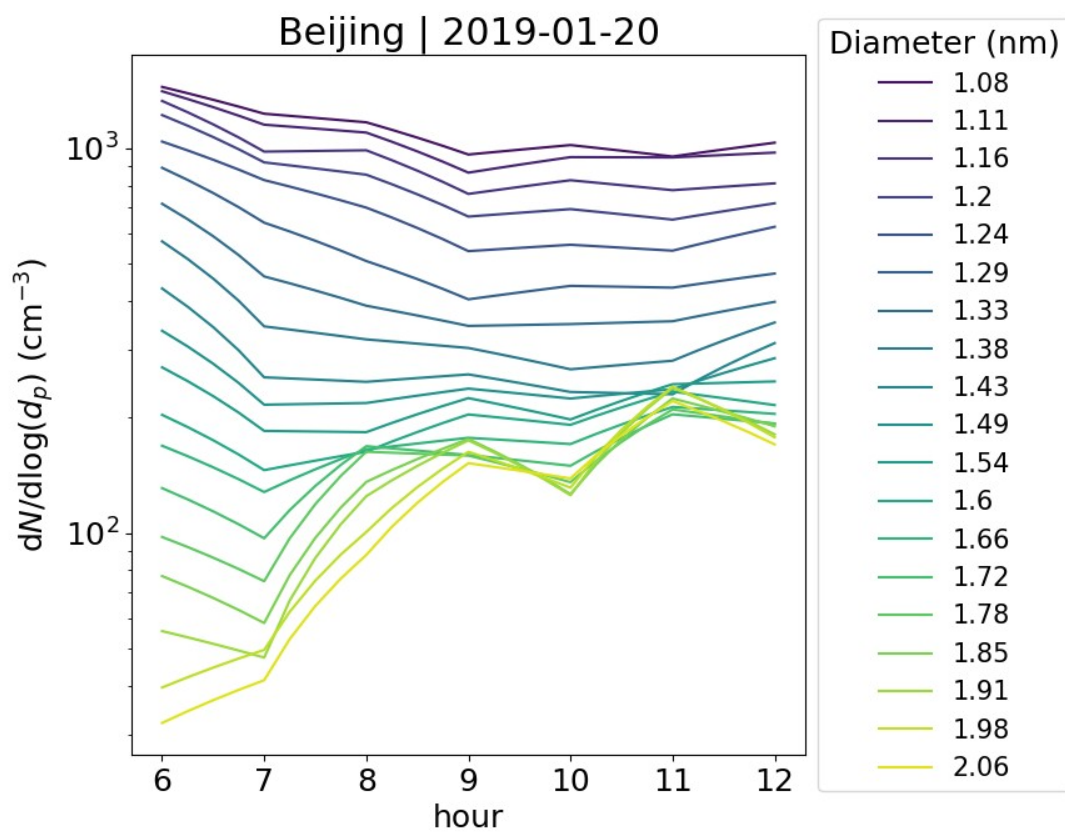
748



749

750 | **Fig. A64:** The upper panels show concentrations of ions of a certain diameter with the hour of the  
 751 day on 10<sup>th</sup> of March, 2021 and 19<sup>th</sup> or April, 2021 in Hyytiälä, Finland. The different colors of the  
 752 line indicate the respective ion diameter ( $d_i$ ). The bottom panels show the appearance time, defined  
 753 as the time that the concentration reaches 50% of its maximum, and the respective  $d_i$ . The ion  
 754 growth rate (GR) derived from these values as a slope of linear regression is shown. For 10<sup>th</sup> of  
 755 March, the GR was determined from 1.24 to 2.05 nm and for 19<sup>th</sup> of April from 1.43 to 2.05 nm.

756



757

758 | **Fig. A75:** The upper panel shows the concentrations of ions of a certain diameter with the hour of  
 759 the day on 20<sup>th</sup> of January, 2019 Beijing, China. The different colors of the line indicate the

760 respective ion diameter ( $d_i$ ). The bottom panel shows the appearance time, defined as the time that  
761 the concentration reaches 50% of its maximum, and the respective  $d_i$ . The ion growth rate (GR)  
762 derived from these values as a slope of linear regression is shown. The GR was determined from  
763 1.72 to 2.06 nm.

## 764 References

- 765 Aalto, P., Hämeri, K., Becker, E., Weber, R., Salm, J., Mäkelä, J. M., Hoell, C., O’ Dowd, C. D.,  
766 Hansson, H.-C., Väkevä, M., Koponen, I. K., Buzorius, G., and Kulmala, M.: Physical  
767 characterization of aerosol particles during nucleation events, *Tellus B*, 53, 344–358,  
768 doi:10.1034/j.1600-0889.2001.530403.x, 2001.
- 769
- 770 Aliaga, D., Tuovinen, S., Zhang, T., Lampilahti, J., Li, X., Ahonen, L., Kokkonen, T., Nieminen, T.,  
771 Hakala, S., Paasonen, P., Bianchi, F., Worsnop, D., Kerminen, V.-M., and Kulmala, M.:  
772 Nanoparticle ranking analysis: determining new particle formation (NPF) event occurrence and  
773 intensity based on the concentration spectrum of formed (sub-5 nm) particles, *Aerosol Research*, 1,  
774 81–92, <https://doi.org/10.5194/ar-1-81-2023>, 2023.
- 775
- 776 Arfin, T., Pillai, A.M., Mathew, N., Tirpude, A, Bang, R., and Mondal, P.: An overview of  
777 atmospheric aerosol and their effects on human health, *Environ Sci Pollut Res* **30**, 125347–125369,  
778 <https://doi.org/10.1007/s11356-023-29652-w>, 2023.
- 779
- 780 Atkinson, R. W., Mills, I. C., Walton, H. A., and Anderson, H. R.: Fine particle components and  
781 health—a systematic review and meta-analysis of epidemiological time series studies of daily  
782 mortality and hospital admissions. *Journal of exposure science & environmental epidemiology*,  
783 25(2), 208–214, <https://doi.org/10.1038/jes.2014.63>, 2015.
- 784
- 785 Bianchi, F., Garmash, O., He, X., Yan, C., Iyer, S., Rosendahl, I., Xu, Z., Rissanen, M. P., Riva, M.,  
786 Taipale, R., Sarnela, N., Petäjä, T., Worsnop, D. R., Kulmala, M., Ehn, M., and Junninen, H.: The  
787 role of highly oxygenated molecules (HOMs) in determining the composition of ambient ions in the  
788 boreal forest, *Atmos. Chem. Phys.*, 17, 13819–13831, <https://doi.org/10.5194/acp-17-13819-2017>,  
789 2017.
- 790
- 791 Boucher, O., Randall, D., Artaxo, P., Bretherton, C., Feingold, G., Forster, P., Kerminen, V.-M.,  
792 Kondo, Y., Liao, H., Lohmann, U., Rasch, P., Satheesh, S., Sherwood, S., Stevens, B., and Zhan, X.:  
793 Clouds and Aerosols, in: *Climate Change 2013: The Physical Science Basis. Contribution of*  
794 *Working Group I to the Fifth Assessment Report of the Intergovernmental Panel on Climate*  
795 *Change*, edited by: Stocker, T., Qin, D., Plattner, G., Tignor, M., Allen, S., Boschung, J., Nauels, A.,  
796 Xia, Y., Bex, V., and Midgley, P., Cambridge University Press, Cambridge, United Kingdom and  
797 New York, NY, USA, 571–657, 10, <https://doi.org/10.1017/CBO9781107415324>, 2013.
- 798
- 799 [Cai, R., Yan, C., Yang, D., Yin, R., Lu, Y., Deng, C., Fu, Y., Ruan, J., Li, X., Kontkanen, J., Zhang,](#)  
800 [Q., Kangasluoma, J., Ma, Y., Hao, J., Worsnop, D. R., Bianchi, F., Paasonen, P., Kerminen, V.-M.,](#)  
801 [Liu, Y., Wang, L., Zheng, J., Kulmala, M., and Jiang, J.: Sulfuric acid–amine nucleation in urban](#)  
802 [Beijing, \*Atmos. Chem. Phys.\*, 21, 2457–2468, <https://doi.org/10.5194/acp-21-2457-2021>, 2021.](#)
- 803
- 804 [Mazon, S.B., Kontkanen, J., Manninen, H. E., Nieminen, T., Kerminen, V. M., and Kulmala, M.: A](#)  
805 [long-term comparison of nighttime cluster events and daytime ion formation in a boreal forest,](#)  
806 [\*Boreal Environ. Res.\*, 21, 242–261, 2016.](#)
- 807

808 Dada, L., Paasonen, P., Nieminen, T., Buenrostro Mazon, S., Kontkanen, J., Peräkylä, O., Lehtipalo,  
809 K., Hussein, T., Petäjä, T., Kerminen, V.-M., Bäck, J., and Kulmala, M.: Long-term analysis of  
810 clear-sky new particle formation events and nonevents in Hyytiälä, *Atmos. Chem. Phys.*, 17, 6227–  
811 6241, <https://doi.org/10.5194/acp-17-6227-2017>, 2017.

812

813 Dal Maso, M., Kulmala, M., Riipinen, I., Wagner, R., Hussein, T., Aalto, P. P., and Lehtinen, K. E.  
814 J.: Formation and growth of fresh atmospheric aerosols: eight years of aerosol size distribution data  
815 from SMEAR II, Hyytiälä, Finland, *Boreal Environ. Res.*, 10, 323–336, 2005.

816

817 Deng, C., Fu, Y., Dada, L., Yan, C., Cai, R., Yang, D., Zhou, Y., Yin, R., Lu, Y., Li, X., Qiao, X.,  
818 Fan, X., Nie, W., Kontkanen, J., Kangasluoma, J., Chu, B., Ding, A., Kerminen, V., Paasonen, P.,  
819 Worsnop, R. D., Bianchi, F., Liu, Y., Zheng, J., Wang, L., Kulmala, M., and Jiang, J.: Seasonal  
820 characteristics of new particle formation and growth in urban Beijing, *Environ. Sci. Technol.*,  
821 54, 8547–8557, <https://doi.org/10.1021/acs.est.0c00808>, 2020.

822

823 Ehn, M., Junninen, H., Petäjä, T., Kurtén, T., Kerminen, V.-M., Schobesberger, S., Manninen, H. E.,  
824 Ortega, I. K., Vehkamäki, H., Kulmala, M., and Worsnop, D. R.: Composition and temporal behavior  
825 of ambient ions in the boreal forest, *Atmos. Chem. Phys.*, 10, 8513–8530, doi:10.5194/acp-10-  
826 8513-2010, 2010.

827

828 Ehn, M., Junninen, H., Schobesberger, S., Manninen, H., Franchin, A., Sipilä, M., Petäjä, T.,  
829 Kerminen, V.-M., Tammet, H., Mirme, A., Mirme, S., Hörrak, U., Kulmala, M., and Worsnop, D.  
830 R.: An instrumental comparison of mobility and mass measurements of atmospheric small ions,  
831 *Aerosol Sci. Tech.*, 45, 522–532, DOI:10.1080/02786826.2010.547890, 2011.

832

833 Fdez-Arroyabe, P., Salcines, C., Kassomenos, P., Santurtún, A., & Petäjä, T.: Electric charge of  
834 atmospheric nanoparticles and its potential implications with human health, *Science of the Total*  
835 *Environment*, 808, 152106, <https://doi.org/10.1016/j.scitotenv.2021.152106>, 2022.

836

837 Finlay, W. H.: Deposition of aerosols in the lungs: Particle characteristics. *Journal of Aerosol*  
838 *Medicine and Pulmonary Drug Delivery*, 34(4), 213–216, doi: 10.1089/jamp.2021.29040.whf,  
839 2021.

840

841 Hari, P. and Kulmala, M.: Station for measuring ecosystem-atmosphere relations, *Boreal Environ.*  
842 *Res.*, 10, 315–322, 2005.

843

844 Harrison, R. G. and Carslaw, K. S.: Ion-aerosol-cloud processes in the lower atmosphere, *Rev.*  
845 *Geophys.*, 41(3), 1012, doi:10.1029/2002RG000114, 2003.

846

847 Harrison, R. G. and Tammet, H.: Ions in Terrestrial Atmosphere and Other Solar System  
848 Atmospheres, *Space Sci. Rev.*, 137, 107–118, DOI 10.1007/s11214-008-9356-x, 2008.

849

850 Hirsikko, A., Laakso, L., Hörrak, U., Aalto, P. P., Kerminen, V.-M. & Kulmala, M.: Annual and  
851 size dependent variation of growth rates and ion concentrations in boreal forest. *Boreal Env. Res.*  
852 10: 357–369, 2005.

853

854 Hirsikko, A., Bergman, T., Laakso, L., Dal Maso, M., Riipinen, I., Hörrak, U., and Kulmala, M.:  
855 Identification and classification of the formation of intermediate ions measured in boreal forest,  
856 *Atmos. Chem. Phys.*, 7, 201–210, <https://doi.org/10.5194/acp-7-201-2007>, 2007.

857

858 Hirsikko, A., Nieminen, T., Gagné, S., Lehtipalo, K., Manninen, H. E., Ehn, M., Hörrak, U.,  
859 Kerminen, V.-M., Laakso, L., McMurry, P. H., Mirme, A., Mirme, S., Petäjä, T., Tammet, H.,  
860 Vakkari, V., Vana, M., and Kulmala, M.: Atmospheric ions and nucleation: a review of observations,  
861 *Atmos. Chem. Phys.*, 11, 767–798, <https://doi.org/10.5194/acp-11-767-2011>, 2011.

862  
863 Hörrak, U., Salm, J., and Tammet, H.: Statistical characterization of  
864 air ion mobility spectra at Tahkuse Observatory: Classification of air ions, *J. Geophys. Res.*, 105,  
865 9291–9302, 2000.

866  
867 Hörrak, U., Aalto, P. P., Salm, J., Komsaare, K., Tammet, H., Mäkelä, J. M., Laakso, L., and  
868 Kulmala, M.: Variation and balance of positive air ion concentrations in a boreal forest, *Atmos.*  
869 *Chem. Phys.*, 8, 655–675, <https://doi.org/10.5194/acp-8-655-2008>, 2008.

870  
871 Jokinen, T., Sipilä, M., Junninen, H., Ehn, M., Lönn, G., Hakala, J., Petäjä, T., Mauldin III, R. L.,  
872 Kulmala, M., and Worsnop, D. R.: Atmospheric sulphuric acid and neutral cluster measurements  
873 using CI-API-TOF, *Atmos. Chem. Phys.*, 12, 4117–4125, <https://doi.org/10.5194/acp-12-4117-2012>,  
874 2012.

875  
876 Kirkby, J., Amorim, A., Baltensperger, U., Carslaw, K. S., Christoudias, T., Curtius, J., Donahue, N.  
877 M., Haddad, I. E., Flagan, R. C., Gordon, H., Hansel, A., Harder, H., Junninen, H., Kulmala, M.,  
878 Kürten, A., Laaksonen, A., Lehtipalo, K., Lelieveld, J., Möhler, O., Riipinen, I., Stratmann, F.,  
879 Tomé, A., Virtanen, A., Volkamer, R., Winkler, P. M., and Worsnop, D. R.: Atmospheric new  
880 particle formation from the CERN CLOUD experiment, *Nat. Geosci.*, 16, 948–957,  
881 <https://doi.org/10.1038/s41561-023-01305-0>, 2023.

882  
883 Kulmala, M., Lehtinen, K. E. J., and Laaksonen, A.: Cluster activation theory as an explanation of  
884 the linear dependence between formation rate of 3nm particles and sulphuric acid concentration,  
885 *Atmos. Chem. Phys.*, 6, 787–793, <https://doi.org/10.5194/acp-6-787-2006>, 2006.

886  
887 Kulmala, M., Riipinen, I., Sipilä, M., Manninen, H., Petaja, T., Junninen, H., Dal Maso, M.,  
888 Mordas, G., Mirme, A., Vana, M., Hirsikko, A., Laakso, L., Harrison, R., Hanson, I., Leung, C.,  
889 Lehtinen, K., and Kerminen, V.: Toward direct measurement of atmospheric nucleation, *Science*,  
890 318, 89–92, doi:10.1126/science.1144124, 2007.

891  
892 Kulmala, M., Petäjä, T., Nieminen, T., Sipilä, M., Manninen, H. E., Lehtipalo, K., Dal Maso, M.,  
893 Aalto, P. P., Junninen, H., Paasonen, P., Riipinen, I., Lehtinen, K. E. J., Laaksonen, A., and  
894 Kerminen, V.-M.: Measurement of the nucleation of atmospheric aerosol particles, *Nat. Protoc.*, 7,  
895 1651–1667, doi:10.1038/nprot.2012091, 2012.

896  
897 Kulmala, M., Kontkanen, J., Junninen, H., Lehtipalo, K., Manninen, H. E., Nieminen, T., Petäjä, T.,  
898 Sipilä, M., Schobesberger, S., Rantala, P., Franchin, A., Jokinen, T., Järvinen, E., Äijälä, M.,  
899 Kangasluoma, J., Hakala, J., Aalto, P. P., Paasonen, P., Mikkilä, J., Vanhanen, J., Aalto, J., Hakola,  
900 H., Makkonen, U., Ruuskanen, T., Mauldin, R. L., Duplissy, J., Vehkamäki, H., Bäck, J.,  
901 Kortelainen, A., Riipinen, I., Kurtén, T., Johnston, M. V., Smith, J. N., Ehn, M., Mentel, T. F.,  
902 Lehtinen, K. E. J., Laaksonen, A., Kerminen, V.-M., and Worsnop, D. R.: Direct Observations of  
903 Atmospheric Aerosol Nucleation, *Science*, 339, 943–946, <https://doi.org/10.1126/science.1227385>,  
904 2013.

905  
906 Kulmala, M., Kerminen, V. M., Petaja, T., Ding, A. J., and Wang, L.: Atmospheric gas-to-particle  
907 conversion: why NPF events are observed in megacities?, *Faraday Discuss.*, 200, 271–288,

908 <https://doi.org/10.1039/c6fd00257a>, 2017.

909

910 Kulmala M., Ezhova E., Kalliokoski T., Noe S., Vesala T., Lohila A., Liski J., Makkonen R., Bäck  
911 J., Petäjä T. and Kerminen V.-M.: CarbonSink+ — Accounting for multiple climate feedbacks from  
912 forests. *Boreal Env. Res.* 25: 145–159, 2020.

913

914 Kulmala, M., Tuovinen, S., Mirme, S., Koemets, P., Ahonen, L., Liu, Y., Junninen, H., Petäjä, T.,  
915 and Kerminen, V.-M.: On the potential of the Cluster Ion Counter (CIC) to observe local new  
916 particle formation, condensation sink and growth rate of newly formed particles, *Aerosol Research*,  
917 2, 291–301, <https://doi.org/10.5194/ar-2-291-2024>, 2024a.

918

919 Kulmala, M., Ke, P., Lintunen, A., Peräkylä, O., Lohtander, A., Tuovinen, S., Lampilahti, J., Kolari,  
920 P., Schiestl-Aalto, P., Kokkonen, T., Nieminen, T., Dada, L., Ylivinkka, I., Petäjä, T., Bäck, J.,  
921 Lohila, A., Heimsch, L., Ezhova, E., and Kerminen, V. M.: A novel concept for assessing the  
922 potential of different boreal ecosystems to mitigate climate change (CarbonSink+ Potential). *Boreal*  
923 *Env. Res.*, 29, 1-16, 2024b.

924

925 Lehtipalo, K., Leppä, J., Kontkanen, J., Kangasluoma, J., Franchin, A., Wimmer, D., Schobesberger,  
926 S., Junninen, H., Petäjä, T., Sipilä, M., Mikkilä, J., Vanhanen, J., Worsnop, D. R., and Kulmala, M.:  
927 Methods for determining particle size distribution and growth rates between 1 and 3 nm using the  
928 Particle Size Magnifier, *Boreal Environ. Res.*, 19, 215–236, 2014.

929

930 Lehtipalo, K., Yan, C., Dada, L., Bianchi, F., Xiao, M., Wagner, R., Stolzenburg, D., Ahonen, L. R.,  
931 Amorim, A., Baccarini, A., Bauer, P. S., Baumgartner, B., Bergen, A., Bernhammer, A.-K.,  
932 Breitenlechner, M., Brilke, S., Buckholz, A., Mazon, S. B., Chen, D., Chen, X., Dias, A., Dommen,  
933 J., Draper, D. C., Duplissy, J., Ehn, M., Finkenzeller, H., Fisher, L., Frege, C., Fuchs, C., Garmash,  
934 O., Gordon, H., Hakala, J., He, X. C., Heikkinen, L., Heinrizi, M., Helm, J. C., Hofbauer, V., Hoyle,  
935 C. R., Jokinen, T., Kangasluoma, J., Kerminen, V.-M., Kim, C., Kirkby, J., Kontkanen, J., Kürten,  
936 A., Lawler, M. J., Mai1, H., Mathot, S., Mauldin III, R. L., Molteni, U., Nichman, L., Nie, W.,  
937 Nieminen, T., Ojdanic, A., Onnela1, A., Passananti, M., Petäjä, T., Piel, F., Pospisilova, V.,  
938 Quéléver, L. L. J., Rissanen, M. P., Rose, C., Sarnela, N., Schallhart, S., Sengupta, K., Simon, M.,  
939 Tauber, C., Tomé, A., Tröst, J., Väisänen, O., Voge, A. L., Volkamer, R., Wagner, A. C., Wang, M.,  
940 Weitz, L., Wimmer, D., Ye, P., Ylisirniö, A., Zha, Q., Carslaw, K., Curtius, J., Donahue, N., Flagan,  
941 R. C., Hansel, A., Riipinen, I., Virtanen, A., Winkler, P. M., Baltensperger, U., Kulmala, M., and  
942 Worsnop, D. R.: Multi-component new particle formation from sulfuric acid, ammonia and biogenic  
943 vapors, *Sci. Adv.*, 4, eaau5363, <https://doi.org/10.1126/sciadv.aau5363>, 2018.

944

945 Li, J., Carlson, B. E., Yung, Y. L., Lv, D., Hansen, J., Penner, J. E., Liao, H., Ramaswamy, V., Kahn,  
946 R. A., Zhang, P., Dubovik, O., Ding, A., Lacis, A. A., Zhang, L., and Dong, Y.: Scattering and  
947 absorbing aerosols in the climate system, *Nature Reviews Earth & Environment*, 3, 363–379,  
948 <https://doi.org/10.1038/s43017-022-00296-7>, 2022.

949

950 Liu, J. Q., Jiang, J. K., Zhang, Q., Deng, J. G., and Hao, J. M.: A spectrometer for measuring  
951 particle size distributions in the range of 3 nm to 10 μm, *Front. Env. Sci. Eng.*, 10, 63–72,  
952 <https://doi.org/10.1007/s11783-014-0754-x>, 2016.

953

954 Liu, Y., Yan, C., Feng, Z., Zheng, F., Fan, X., Zhang, Y., Li, C., Zhou, Y., Lin, Z., Guo, Y., Zhang,  
955 Y., Ma, L., Zhou, W., Liu, Z., Dada, L., Dällenbach, K., Kontkanen, J., Cai, R., Chan, T., Chu, B.,  
956 Du, W., Yao, L., Wang, Y., Cai, J., Kangasluoma, J., Kokkonen, T., Kujansuu, J., Rusanen, A., Deng,  
957 C., Fu, Y., Yin, R., Li, X., Lu, Y., Liu, Y., Lian, C., Yang, D., Wang, W., Ge, M., Wang, Y., Worsnop,

958 D. R., Junninen, H., He, H., Kerminen, V.-M., Zheng, J., Wang, L., Jiang, J., Petäjä, T., Bianchi, F.,  
959 and Kulmala, M.: Continuous and comprehensive atmospheric observations in Beijing: a station to  
960 understand the complex urban atmospheric environment, *Big Earth Data*, 4, 295–321,  
961 <https://doi.org/10.1080/20964471.2020.1798707>, 2020.

962  
963 [Mazon, S.B., Kontkanen, J., Manninen, H. E., Nieminen, T., Kerminen, V.-M., and Kulmala, M.: A](#)  
964 [long-term comparison of nighttime cluster events and daytime ion formation in a boreal forest,](#)  
965 [\*Boreal Environ. Res.\*, 21, 242–261, 2016.](#)

966  
967 Mirme, S. and Mirme, A.: The mathematical principles and design of the NAIS – a spectrometer for  
968 the measurement of cluster ion and nanometer aerosol size distributions, *Atmos. Meas. Tech.*, 6,  
969 1061–1071, <https://doi.org/10.5194/amt-6-1061-2013>, 2013.

970  
971 Mirme, S., Balbaaki, R., Manninen, H. E., Koemets, P., Sommer, E., Rörup, B., Wu, Y., Almeida, J.,  
972 Ehrhart, S., Weber, S. K., Pfeifer, J., Kangasluoma, J., Kulmala, M., and Kirkby, J.: Design and  
973 performance of the Cluster Ion Counter (CIC), *Atmos. Meas. Tech. Discuss.* [preprint],  
974 <https://doi.org/10.5194/amt-2024-138>, accepted for publication, 2024.

975  
976 Quaas, J., Ming, Y., Menon, S., Takemura, T., Wang, M., Penner, J.E., Gettelman, A., Lohmann, U.,  
977 Bellouin, N., Boucher, O., Sayer, A.M., Thomas, G.E., McComiskey, A., Feingold, G., Hoose, C.,  
978 Kristjánsson, J.E., Liu, X., Balkanski, Y., Donner, L. J., Ginoux, P.A., Stier, P., Grandey, B.,  
979 Feichter, J., Sednev, I., Bauer, S.E., Koch, D., Grainger, R.G., Kirkevåg, A., Iversen, T., Seland, Ø.,  
980 Easter, R., Ghan, S.J., Rasch, P.J., Morrison, H., Lamarque, J.-F., Iacono, M. J., Kinne, S., and  
981 Schulz, M.: Aerosol indirect effects – general circulation mode intercomparison and evaluation with  
982 satellite data, *Atmos. Chem. Phys.*, 9, 8697–8717, doi:10.5194/acp-9-8697-2009, 2009.

983  
984 [Quéléver, L. L. J., Kristensen, K., Normann Jensen, L., Rosati, B., Teiwes, R., Daellenbach, K. R.,](#)  
985 [Peräkylä, O., Roldin, P., Bossi, R., Pedersen, H. B., Glasius, M., Bilde, M., and Ehn, M.: Effect of](#)  
986 [temperature on the formation of highly oxygenated organic molecules \(HOMs\) from alpha-pinene](#)  
987 [ozonolysis, \*Atmos. Chem. Phys.\*, 19, 7609–7625, <https://doi.org/10.5194/acp-19-7609-2019>, 2019.](#)

988  
989 Rose, C., Zha, Q., Dada, L., Yan, C., Lehtipalo, K., Junninen, H., Mazon, S. B., Jokinen, T., Sarnela,  
990 N., Sipilä, M., Petäjä, T., Kerminen, V.-M., Bianchi, F., and Kulmala, M.: Observations of biogenic  
991 ion-induced cluster formation in the atmosphere, *Sci. Adv.*, 4, 1–11, DOI:[10.1126/sciadv.aar5218](https://doi.org/10.1126/sciadv.aar5218),  
992 2018.

993  
994 [Zha, Q., Huang, W., Aliaga, D., Peräkylä, O., Heikkinen, L., Koenig, A. M., Wu, C., Enroth, J.,](#)  
995 [Gramlich, Y., Cai, J., Carbone, S., Hansel, A., Petäjä, T., Kulmala, M., Worsnop, D., Sinclair, V.,](#)  
996 [Krejci, R., Andrade, M., Mohr, C., and Bianchi, F.: Measurement report: Molecular-level](#)  
997 [investigation of atmospheric cluster ions at the tropical high-altitude research station Chacaltaya](#)  
998 [\(5240 m a.s.l.\) in the Bolivian Andes, \*Atmos. Chem. Phys.\*, 23, 4559–4576,](#)  
999 [<https://doi.org/10.5194/acp-23-4559-2023>, 2023.](#)

1000  
1001 Schmale, J., Zieger, P., and Ekman, A. M. L.: Aerosols in current and future Arctic climate, *Nat.*  
1002 *Clim. Change*, 11, 95–105, <https://doi.org/10.1038/s41558-020-00969-5>, 2021.

1003  
1004 Shiraiwa, M., Ueda, K., Pozzer, A., Lammel, G., Kampf, C. J., Fushimi, A., Enami, S., Arangio, A.  
1005 M., Fröhlich-Nowoisky, J., Fujitani, Y., Furuyama, A., Lakey, P. S. J., Lelieveld, J., Lucas, K.,  
1006 Morino, Y., Pöschl, U., Takahama, S., Takami, A., Tong, H., Weber, B., Yoshino, A., and Sato, K.:

- 1007 Aerosol health effects from molecular to global scales, *Environ. Sci. Technol.*, 51, 13545–13567,  
1008 <https://doi.org/10.1021/acs.est.7b04417>, 2017.
- 1009
- 1010 Shuman, N. S., Hunton, D. E., and Viggiano, A. A.: Ambient and modified atmospheric ion  
1011 chemistry: from top to bottom, *Chem. Rev.*, 115, 4542–4570, <https://doi.org/10.1021/cr5003479>,  
1012 2015.
- 1013
- 1014 Sulo, J., Sarnela, N., Kontkanen, J., Ahonen, L., Paasonen, P., Laurila, T., Jokinen, T.,  
1015 Kangasluoma, J., Junninen, H., Sipilä, M., Petäjä, T., Kulmala, M., and Lehtipalo, K.: Long-term  
1016 measurement of sub-3 nm particles and their precursor gases in the boreal forest, *Atmos. Chem.*  
1017 *Phys.*, 21, 695–715, <https://doi.org/10.5194/acp-21-695-2021>, 2021.
- 1018
- 1019 Tammet, H.: Size and mobility of nanometer particles, clusters and ions, *J. Aerosol Sci.*, 26, 459–  
1020 475, 1995.
- 1021
- 1022 Tammet, H., Hörrak, U., Laakso, L., and Kulmala, M.: Factors of air ion balance in a coniferous  
1023 forest according to measurements in Hyytiälä, Finland, *Atmos. Chem. Phys.*, 6, 3377–3390,  
1024 <https://doi.org/10.5194/acp-6-3377-2006>, 2006.
- 1025
- Tammet, H., Komsaare, K., and Horrak, U.: Intermediate ions in the atmosphere, *Atmos. Res.*, 135-  
136, 263-273, <https://doi.org/10.1016/j.atmosres.2012.09.009>, 2014.
- Tuovinen, S., Lampilahti, J., Kerminen, V.-M., and Kulmala, M.: Intermediate ions as indicator for  
local new particle formation, *Aerosol Research*, 2, 93–105, <https://doi.org/10.5194/ar-2-93-2024>,  
2024.
- Wagner, R., Manninen, H. E., Franchin, A., Lehtipalo, K., Mirme, S., Steiner, G., Petäjä, T., and  
Kulmala, M.: On the accuracy of ion measurements using a Neutral cluster and Air Ion  
Spectrometer, *Boreal Env. Res.*, 21, 230–241, 2016
- Yan, C., Yin, R., Lu, Y., Dada, L., Yang, D., Fu, Y., Kontkanen, J., Deng, C., Garmash, O., Ruan, J.,  
Baalbaki, R., Schervish, M., Cai, R., Bloss, M., Chan, T., Chen, T., Chen, Q., Chen, X., Chen, Y.,  
Chu, B., Dällenbach, K., Foreback, B., He, X., Heikki-nen, L., Jokinen, T., Junninen, H.,  
Kangasluoma, J., Kokkonen, T., Kurppa, M., Lehtipalo, K., Li, H., Li, H., Li, X., Liu, Y., Ma, Q.,  
Paasonen, P., Rantala, P., Pileci, R. E., Rusanen, A., Sarnela, N., Simonen, P., Wang, S., Wang, W.,  
Wang, Y., Xue, M., Yang, G., Yao, L., Zhou, Y., Kujansuu, J., Petäjä, T., Nie, W., Ma, Y., Ge, M.,  
He, H., Donahue, N. M., Worsnop, D. R., Veli-Matti, K., Wang, L., Liu, Y., Zheng, J., Kulmala, M.,  
Jiang, J., and Bianchi, F.: The Synergistic Role of Sulfuric Acid, Bases, and Oxidized Organics  
Governing New-Particle Formation in Beijing, *Geophys. Res. Lett.*, 48, e2020GL091944,  
<https://doi.org/10.1029/2020gl091944>, 2021.
- [Yao, L., Garmash, O., Bianchi, F., Zheng, J., Yan, C., Kontkanen, J., Junninen, H., Mazon, S. B., Ehn, M., Paasonen, P., Sipilä, M., Wang, M., Wang, X., Xiao, S., Chen, H., Lu, Y., Zhang, B., Wang, D., Fu, Q., Geng, F., Li, L., Wang, H., Qiao, L., Yang, X., Chen, J., Kerminen, V.-M., Petäjä, T., Worsnop, D. R., Kulmala, M., and Wang, L.: Atmospheric new particle formation from sulfuric acid and amines in a Chinese megacity, \*Science\*, 361, 278–281, <https://doi.org/10.1126/science.aao4839>, 2018.](#)
- Yli-Juuti, T., Nieminen, T., Hirsikko, A., Aalto, P. P., Asmi, E., Hörrak, U., Manninen, H. E.,  
Patokoski, J., Dal Maso, M., Petäjä, T., Rinne, J., Kulmala, M., and Riipinen, I.: Growth rates of  
nucleation mode particles in Hyytiälä during 2003–2009: variation with particle size, season, data

analysis method and ambient conditions, *Atmos. Chem. Phys.*, 11, 12865–12886, <https://doi.org/10.5194/acp-11-12865-2011>, 2011.

1026 |

1027 |

1028 |

1029 |